Turkish Journal of Earth Sciences (Turkish J. Earth Sci.), **Vol. 16**, 2007, pp. 493–522. *Copyright ©TÜBİTAK*

The Dikili-Çandarlı Volcanics, Western Turkey: Magmatic Interactions as Recorded by Petrographic and Geochemical Features

ZEKİYE KARACIK[1], YÜCEL YILMAZ[2] & JULIAN A. PEARCE[3]

[1] İstanbul Technical University, Faculty of Mines, Department of Geology, Ayazağa, TR–34469 İstanbul, Turkey
(E-mail: zkaracik@itu.edu.tr)
[2] Kadir Has University, Cibali Merkez Kampüsü, Cibali, TR–34230 İstanbul, Turkey
[3] Cardiff University, Department of Earth, Ocean and Planetary Science, Cardiff, UK

Abstract: Located in the northwestern part of the Aegean region, Dikili-Çandarlı volcanic suite contains products representative for the western Anatolian Miocene volcanism. They can be divided into two main groups: the Dikili and the Çandarlı groups. The Dikili group is Early–Middle Miocene in age and consists mainly of pyroclastic rocks, andesitic-dacitic lavas, lava breccia, lahar flows and associated sedimentary rocks. The lavas contain disequilibrium phenocrysts assemblages. The Çandarlı group consists of Upper Miocene–Pliocene lava and sediment associations. The volcanic rocks consist mainly of rhyolitic domes and basaltic trachyandesite-basaltic andesite lavas erupted along the NW–SE- and NE–SW-trending fault systems; the faults controlled the development of the Çandarlı depression.

Major- and trace-element chemistry indicates that the lavas are dominantly high-K, calc-alkaline, intermediate to acidic in composition. Chemical and textural characteristics of the minerals reveal that mixing was a common process in the generation of this magma. In particular, petrography, textural evidence and crystal chemistry of the phenocrysts together with variations in rock compositions indicate that basaltic-basaltic andesitic magma intruded dacite magma and is partially hybridized with it.

New petrographic and geochemical data of Dikili-Çandarlı volcanics are closely similar to those of the active continental margin volcanism which are interpreted as mantle-derived magmas contaminated by crustal materials.

Key Words: volcanism, geochemistry, mineral chemistry, mixing, Turkish Aegean region

Dikili-Çandarlı (Batı Anadolu) Volkaniklerindeki Magmatik Etkileşimlerin Petrografik ve Jeokimyasal Özellikleri

Özet: Ege Bölgesinin kuzeybatısında yeralan Dikili-Çandarlı volkanikleri Miyosen yaşlı Batı Anadolu volkanizmasının temsilci örneğini oluşturur. Volkanikler, Dikili ve Çandarlı grubu olarak iki ana gruba ayrılırlar. Erken–Orta Miyosen yaşlı Dikili grubu başlıca piroklastik birimler, andezitik, dasitik lavlar, lav breşleri, lahar akıntıları ve bunlarla ilişkili çökel kayalardan oluşur. Lavlar dengesiz fenokristal toplulukları içermektedir. Geç Miyosen–Pliyosen yaşlı Çandarlı grubu ise çökel topluluk ile riyolitik domlar ve Çandarlı çöküntüsünü oluşturan KB–GD- ve KD–GB-gidişli fay sistemleri boyunca püskürmüş bazaltik trakiandezitik-bazaltik andezitik lavlardan oluşur.

Ana ve iz element kimyası lavların çoğunlukla yüksek-K'lu, kalkalkalin, ortaç-asidik bileşimli olduğunu göstermektedir. Minerallerin kimyasal ve dokusal özellikleri magma gelişimi sırasında karışma işlemlerinin yaygın olarak geliştiğini göstermektedir. Özellikle fenokristallerin petrografik, dokusal özellikleri ve kristal kimyası ile tüm kayaç bileşimleri birarada değerlendirildiğinde bazaltik-bazaltik andezitik magmanın dasitik bir magma içine sokulduğu ve birlikte melezleştiği anlaşılmaktadır.

Dikili-Çandarlı volkaniklerinin yeni petrografik ve jeokimyasal verileri bunların aktif kıta kenarı volkaniklerine benzerlik gösterdiğini ve manto kaynaklı bir magmanın kabuksal malzemeler ile kirlenmesi sonucu geliştiğini göstermektedir.

Anahtar Sözcükler: volkanizma, jeokimya, mineral kimyası, magma karışımı, Ege bölgesi

Introduction

Widespread magmatism closely related to the tectonic evolution of the western Anatolia produced both intrusive and extrusive rocks during the Eocene–Pliocene period. Paleocene continental collision between the Anatolide-Tauride block and the Sakarya Continent along the İzmir-Ankara suture resulted in crustal thickening and shortening (e.g., Şengör & Yılmaz 1981). The northerly

subduction of the Neotethys Ocean during the Late Cretaceous–Eocene period and the subsequent collision produced the initial stage of widespread magmatism in western Turkey (e.g., Innocenti *et al.* 1982; Yılmaz 1989; Güleç 1991; Karacık & Yılmaz 1998; Aldanmaz *et al*. 2000; Yılmaz *et al*. 2001; Erkül *et al*. 2005a). These magmatic rocks are late/post collisional with respect to the Tethyan collision, commonly high-K, calc-alkaline, partly shoshonitic and hybrid geochemically. The second stage is related to the N–S extensional tectonic regime, which has been affecting the Aegean region since the latest Oligocene–Early Miocene (Borsi *et al.* 1972; Innocenti *et al.* 1982; Yılmaz 1989; Savaşçın 1990; Güleç 1991; Seyitoğlu *et al.* 1997; Aldanmaz *et al*. 2000; Yılmaz *et al*. 2001; Aldanmaz 2002, 2006; Alıcı *et al.* 2002; Tokçaer *et al.* 2005; Erkül *et al.* 2005b; Yücel-Öztürk *et al.* 2005). The products of this period are mainly alkali basalts and basanites.

The Dikili-Çandarlı high is a mountainous terrain located on the western tip of the Bakırçay Graben. The region is delimited by two sets of oblique-slip faults trending in NE–SW and NW–SE direction. All the products of the calc-alkaline Miocene volcanism of western Anatolia crop out in this area. Although, there are limited number of studies on this area (Öngür 1972; Kozan *et al.* 1982; Akyürek & Soysal 1983; Ercan & Günay 1984) and no detailed study has yet been done; only the high-K calk-alkaline character (Borsi *et al.* 1972; Ercan & Günay 1984; Aldanmaz *et al.* 2000) has already been mentioned. Mineral chemistry of Early–Middle Miocene calc-alkaline volcanism in western Anatolia is reported by recent work of Aldanmaz (2006). He estimated the pre-eruption temperature and pressure of the Miocene volcanic rocks.

Geochemical investigations of calc-alkaline lavas and plutons have suggested that mixing of contrasting magmas can account for the compositional features of many co-magmatic suites (cf. Eichelberger 1975; Anderson 1976; Langmuir *et al.* 1978; Murphy *et al.* 2000). Magma mixing has been shown to be an important process among intermediate magmas in many tectonic settings for instance Montserrat (Steward & Fowler 2001), Lassen Peak (California: Clynne 1999), Chaos Crags (California: Tepley *et al.* 1999) and mineralogical disequilibrium may be the only direct evidence for a mixing origin. So, mineral analyses are an invaluable tool for studying the evolution of andesitic lavas. Mineral textures, zoning patterns – mostly feldspar zoning – and reaction textures from andesite to dacite lavas sensitively register magma mixing processes and shifting magmatic conditions.

The objective of this research is to determine volcanic evolution of the Dikili-Çandarlı area and to document the evidences as regards to the nature of magma source(s) and the effects of magma mixing and fractional crystallization, by using mineralogical, petrological and geochemical approaches. For this reason, new field data derived from a detailed mapping of the region are complemented by thorough petrological studies. Based on these studies, we attempted to reconstruct the overall development of the Dikili-Çandarlı volcanic complex and to present a tentative petrogenetic model for the magmas.

Geological Setting

The Dikili-Çandarlı high consists essentially of volcanic rocks. Two major rock groups have been distinguished: the Dikili and the Çandarlı groups (Karacık & Yılmaz 2000) (Figure 1). The Dikili group is Early–Middle Miocene in age, and consists mainly of pyroclastic rocks, lavas and associated sedimentary rocks. The Çandarlı group consists of Upper Miocene–Pliocene sediment association and volcanic rocks, which are rhyolitic domes and basaltic andesite-basalt lavas-dikes. The contact between Dikili and Çandarlı groups is an unconformity surface.

Dikili Group

The Dikili group consists mainly of pyroclastic rocks and lava flows (Figure 1). The first products are pyroclastic rocks represented by fall and flow deposits that pass laterally and vertically into lavas. The fall-out deposits are widespread in the eastern part of the study area and consist of ash fall, pumice and ash fall, ash and block fall deposits displaying well-developed bedding planes. Explosive activity appears to have been either plinian or sub-plinian type. Lithic fragments range from 0.5 to 1.0 cm in diameter. The pyroclastic flow deposits are either block and ash flow or pumice flows, mostly thin and internally chaotic. Their fragments are andesitic and latitic in composition and medium to coarse grained. The matrix is of ash, dust and pumice.

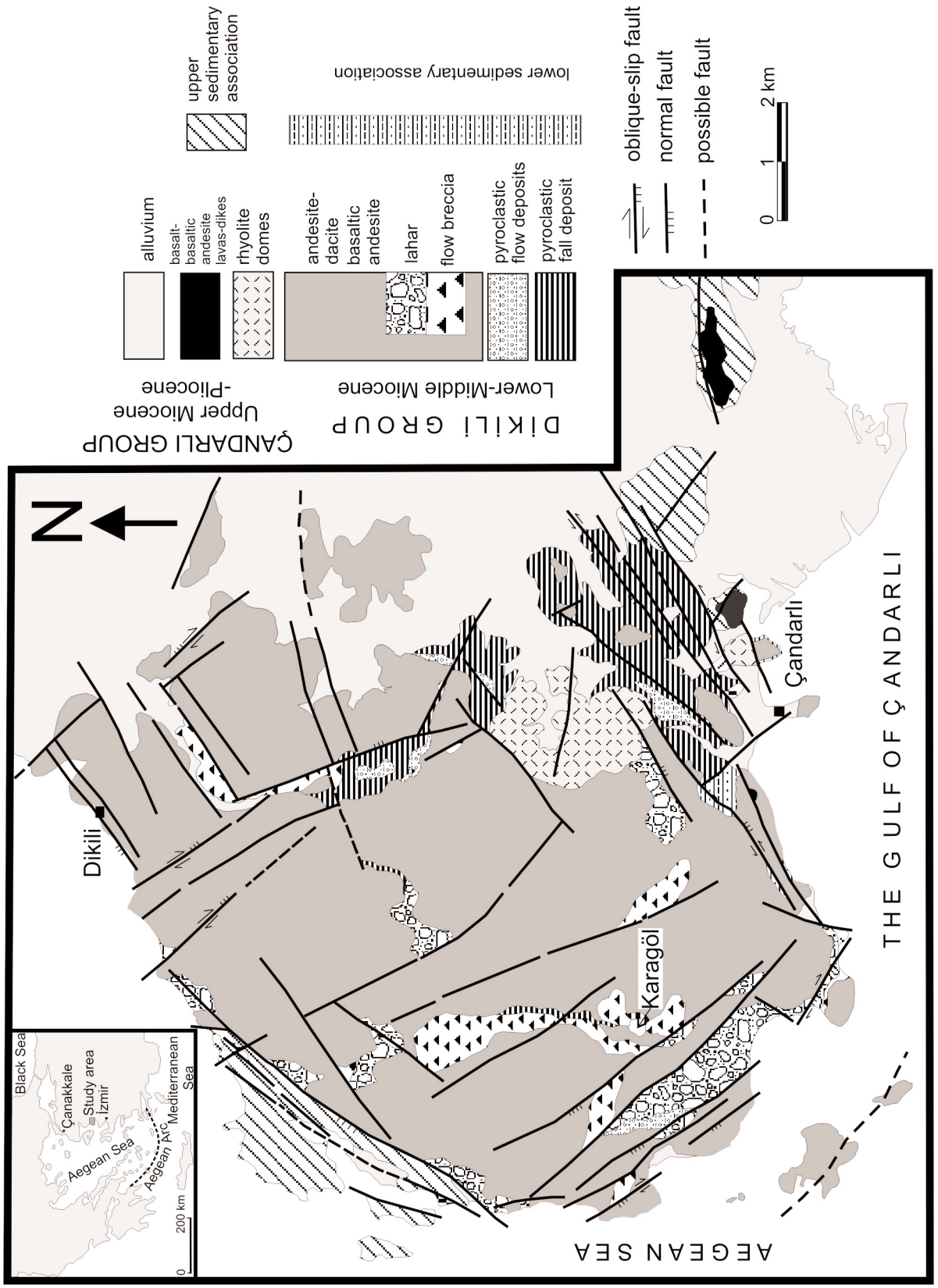

Figure 1. Geological map of the Dikili-Çandarlı region.

The intercalated sedimentary rocks form the lower sedimentary association. They are limited in extent and consist mainly of volcanogenic mudstone, siltstone, sandstone, reworked tuff and occasional conglomerates. This sedimentary unit is widespread in Western Anatolia, and is known as Küçükkuyu formation in the Edremit Graben (Siyako *et al.* 1989; Ediger *et al.* 1996; Karacık & Yılmaz 1998), Evrenli formation around the Gediz Graben (İztan & Yazman 1990; Ediger *et al.* 1996), and lower sedimentary association in the Zeytindağ region (Genç & Yılmaz 2000).

Lavas, lava breccia and laharic flows overlying the basal pyroclastic rocks form the bulk of the Dikili group and alternate with one another at all levels. The flow breccias are commonly located at the top of the lavas and are composed of andesitic-dacitic sub-angular to angular lava fragments entrapped within lava matrix. Their size varies from 2 to 40 cm, but may reach up to 1 m in some places.

The most common lithologies of the Dikili group are andesite and dacite lava flows and stocks. They, particularly crystal-rich dacitic lavas, display locally well-developed flow foliation and bear dioritic and micro-dioritic xenoliths. Ubiquitous minerals are plagioclase, quartz, hornblende, pyroxene and biotite. The matrix is commonly microlithic and cryptocrystalline.

Four different explosion stages separated by palaeosol surfaces may be distinguished within the volcanic pile. Several faults post-dating the volcanism considerably changed the original morphology. Even so, its morphological and lithological features are relatively well preserved around the lake Karagöl (Figure 1), 500 m above the sea level and about 250 m across, where the centre of the explosion is still recognizable. The lava flows radiate away from the lake centre. In this location the lake corresponds to the crater lake.

Radiometric dating on intermediate lavas of the Dikili group yielded Early to Middle Miocene age (16.7–18.5 Ma: Borsi *et al.* 1972; Benda *et al.* 1974; 15.2±0.40–15.5±0.30: Aldanmaz *et al.* 2000) Palaeontological ages from the sediments intercalated with the volcanic rocks are in agreement with the radiometric ages (Borsi *et al.* 1972; Benda *et al.* 1974; Krusensky 1976; Ercan *et al.* 1984, 1996; Ediger *et al.* 1996; Seyitoğlu *et al.* 1997).

Çandarlı Group

Sedimentary and volcanic rocks of the Çandarlı group formed during the Late Miocene–Early Pliocene period (Figure 1). The sedimentary rocks rest unconformably on the underlying volcanic succession and begin with grey-green shales, followed by sandstone, marl, and siltstone alternation; the sequence then passes upward into white limestones. This unit apparently deposited in a low-energy lacustrine environment is also an extensive unit and is known alternatively as Urla limestone in the Karaburun peninsula (Kaya 1981), Yeniköy formation around the Seferihisar (Genç *et al.* 2001), and Ularca limestone in the northern part of the Bakırçay Graben (Yılmaz *et al.* 2000). A second volcanic episode producing mafic and felsic lavas began partly simultaneously with the development of this sedimentary unit. Mafic lavas, basaltic andesite and basaltic trachyandesite, were erupted along the margin-bounding faults of the Çandarlı depression (Figure 1). At the bottom, the mafic lava flows are commonly brecciated; at higher levels they display well-developed columnar jointing.

The late products of the second volcanic activity are fall deposits, rhyolitic volcanic domes and a pumice cone. Obsidian and/or perlite are also common. These viscous lavas did not travel far away from the volcanic centre. Generally they are located along the NW–NE-trending fault zones accumulating around the fissure and forming a more than 150-m-thick stout dome (Figure 1), cutting across co-genetic fall deposits. Flow bedding is vertical at the centre of the dome, but away from the centre the lavas exhibit well-developed flow foliations. High degrees of vesiculation are indicated by vesicles in the dome centres, which vary in size from 20 cm to 2 m. Apparently, the volcanic edifice was extruded as froth flow at some stage. Pumice cone consists of mainly pumice and decreasing amount of ash and lithic fragments, which form outward dipping walls.

Analytical Techniques

Minerals were analyzed using an electron-scanning microscope. Thin sections were prepared and carbon coated at Cardiff University and analyzed on Cambridge Instruments (LEO) S360. The standards for silicate analyses are Na- Albite, Mg- MgO, Al–Al_2O_3, Si- SiO_2, K - Orthoclase, Ca- Wollastonite, and Mn, Fe, etc. are pure metals.

Major and trace elements were determined at Cardiff University. Samples were ignited at 900 °C in a muffle furnace to determine loss on ignition. 0.1 grams of ignited powder were fused with 0.4 grams of Li-metaborate and the resulting melts were dissolved and taken up in 100 ml of 2% HNO_3. Sample solutions were analyzed by inductively coupled plasma-optical emission spectrometry (ICP-OES) using a JY Horiba Ultima 2 ICP-OES system. Analytical lines used were as follows: P, 214.91 nm; Ni, 216.56 nm; Co, 228.62 nm; Ba, 233.53 nm; Si, 251.61 nm; Mn, 257.61 nm; Fe, 259.94 nm; Cr, 267.72 nm; Mg, 279.55 nm; Al, 308.21 nm; V, 310.23 nm; Ca, 422.67 nm; Cu, 324.75 nm; Ti, 334.94 nm; Zr, 343.82 nm; Sc 361.38 nm; Y, 371.03 nm; Sr, 407.77 nm; Na 588.99 nm; and K, 766.49 nm. Calibration was performed by external calibration using solutions prepared from the international reference materials BIR-1, W2, MRG-1, JA2 and JG3 in the same manner as above. Instrumental precision varied between 0.2–8.5 percent depending on the elemental concentration present. Accuracy was determined by repeat analysis of separate (user-prepared) solutions of W2 and JA2 and of the international granite standard GSP-1. Results were consistently within 5% of the accepted values.

Petrography and Mineral Chemistry

Dikili Group

Lavas of the Dikili group range from aphyric to highly porphyritic with up to 40–55 wt% rarely 20–30 wt% phenocrysts, micro-phenocrysts and microlites. The porphyritic lavas contain coarse phenocrysts of plagioclase (50–60%), clinopyroxene (5–15%), hornblende (5–10%), orthopyroxene (1–5%), quartz (1%) or olivine (1%). Apatite, magnetite and ilmenite occur in trace amounts.

Porphyritic, pilotaxitic and glomeroporphyritic texture are typical in the rocks of this group. The most common type of crystal clots consists of euhedral plagioglase and oxides complexly intergrown with euhedral to subhedral clinopyroxene, orthopyroxene, or both. The groundmass of the andesites is microlitic or microcrystalline. Dacites have vitrophyric, felcitic, or spherulitic quartz-feldspar groundmass. Needle-like secondary crystallisation forming flow bands is common. Representative chemical analyses of the main minerals of the Dikili and Çandarlı group lavas are given in Tables 1–6.

Plagioclase is the principal mineral in all andesite-dacite from the Dikili group. It ranges in size from small microlites to large phenocrysts, which are all twined and zoned and have compositions ranging from An_{79} to An_{35}. Zonal arrangements of melt inclusions and minerals (biotite, pyroxene) are common either parallel to the cleavage or cumulate centre of the crystals. Three main plagioclase populations are distinguished on the basis of composition, zoning patterns and textures (Tables 1 & 2). (Figure 2): (i) normally-zoned phenocrysts typically have cores between An_{66} and An_{44} and rims between An_{58} and $An_{26;}$ (ii) reversely-zoned large phenocrysts have

Table 1. Compositional differences of the plagioclase minerals in Dikili and Çandarlı lavas. (C) core, (R) rim of the zoned mineral, WZ– weakly zoned, NZ– normal zoned.

Sample no	Rock type		Phenocrystal	Normal zoning	Reverse zoning	Pachy zoning	Microlite
Zk-40	basaltic andesite	Çandarlı group	An_{61-77}	X	X	X	X
Zk-70	andesite	Çandarlı group	An_{45}	C: An_{81}-R: An_{47}	C: An_{80}-R: An_{85}	X	X
Zk-90	andesite	Dikili group	An_{50-66}	C: An_{66}-R: An_{58}	C: An_{58}-R: An_{68}	X	An_{59}
Zk-64	andesite	Dikili group	An_{46-63}	C: An_{47}-R: An_{42}	C: An_{46}-R: An_{60}	An_{64-69}	An_{51}
Zk-83	dacite	Dikili group	X	C: An_{51}-R: An_{42}	C: An_{40}-R: An_{64}	An_{43-62}	X
Zk-23	dacite	Dikili group	An_{35-45}	X	X	X	An_{59}
Zk-29	dacite	Dikili group	An_{35-54}	C: An_{56}-R: An_{48}	X	X	An_{56}
Zk-69	rhyolite	Dikili group		C: An_{44}-R: An_{26}		Al rich outher zone	
						An_{30}	An_{49}
Zk-74	rhyolite	Dikili group	An_{17-20}	WZ.C: An_{24}-R: An_{20}			
				NZ.C: An_{34}-R: An_{17}			

Table 2. Representative plagioclase analyses of the Dikili and Çandarlı lavas. Structural formulae of the feldspars on the basis of 8 oxygens.

Sample no	83.6 core	83.6.1 rim	83.6.3 core	83.6.6 rim	83.7.4 core	83.7.3 pachy zone	83.7.2 rim	83.5.1 core	83.5.2 parch zone	83.5.3 rim
SiO_2	55.34	58.07	55.02	53.04	58.16	58.25	52.59	58.43	57.36	52.09
TiO_2	0.03	0.06	0	0	0.16	0.05	0	0.05	0	0.01
Al_2O_3	27.53	24.96	27.5	28.74	25.65	26.29	29.22	25.63	26.68	30.23
FeO	0.24	0.32	0.31	0.67	0.35	0.4	0.73	0.32	0.31	0.54
CaO	10.6	7.7	10.74	12.61	8.4	8.9	12.93	8.31	9.68	13.9
Na_2O	5.66	6.93	5.72	4.54	6.64	6.41	4.42	6.69	6.26	4.09
K_2O	0.52	0.97	0.5	0.5	0.74	0.79	0.41	0.81	0.63	0.27
MgO	0	0	0	0.02	0	0	0	0	0	0
BaO	0	0.15	0.11	0.3	0	0	0.01	0.11	0.1	0.09
Total	99.92	99.16	99.9	100.42	100.1	101.09	100.31	100.35	101.02	101.22
An	50.8	38.0	50.9	60.5	41.1	43.4	61.8	40.7	46.1	65.2
Al	49.2	62.0	49.1	39.5	58.9	56.6	38.2	59.3	53.9	34.8

Sample no	83.2.1	83.2.2	83.2.3	83.3.1 core	83.3.2 rim
SiO_2	58.92	57.53	58.48	57.59	51.87
TiO_2	0.1	0.09	0	0	0.07
Al_2O_3	25.7	25.45	24.89	25.18	28.94
FeO	0.26	0.31	0.29	0.27	0.55
CaO	8.32	8.59	7.74	8.43	13.35
Na_2O	6.92	6.55	6.81	6.88	4.2
K_2O	0.81	0.73	0.89	0.71	0.32
MgO	0	0	0	0	0
BaO	0	0	0.15	0.08	0
Total	101.03	99.25	99.25	99.14	99.3
An	39.9	42.0	38.6	40.4	63.7
Al	60.1	58.0	61.4	59.6	36.3

Sample no	s90.1 core	s90.2 rim	s90.3 core	s90.4 rim	s90.9 microlite	s90.21 core	s90.22 rim	s90.26 core	s90.27 rim
Na_2O	3.89	3.08	4.06	5.39	5.15	4.4	4.99	3.42	4.46
Al_2O_3	15.24	31.4	30.15	27.67	27.7	29.44	28.64	30.25	28.99
SiO_2	33.63	49.3	51.74	55.08	54.95	52.9	54.2	50.58	52.95
K_2O	0.18	0.08	0.22	0.53	0.48	0.3	0.39	0.21	0.35
CaO	5.3	15.89	13.82	11.52	11.4	13.42	12.04	14.81	13.04
TiO_2	0.02	0.03	0.01	0.07	0.07	0	0.06	0.12	0.01
FeO	0.25	0.54	0.53	0.7	0.6	0.41	0.46	0.49	0.58
Total	58.5	100.32	100.53	100.96	100.35	100.87	100.77	99.88	100.37
An	43.0	74.0	65.3	54.2	55.0	62.8	57.1	70.5	61.8
Al	57.0	26.0	34.7	45.8	45.0	37.2	42.9	29.5	38.2

Table 2. Continued.

Sample no	s90.28 core	s90.29 rim	s90.30 core	s90.31 rim	s90.34 core	s90.35 rim	s90-p1 microlite	s90-p2
Na_2O	6.09	5.05	4.48	4.69	5.61	4.41	4.58	3.96
Al_2O_3	26.19	28.19	29.18	28.35	26.94	29.02	28.65	29.7
SiO_2	56.81	54.7	52.58	53.14	55.36	52.7	52.51	51.23
K_2O	0.68	0.39	0.25	0.33	0.46	0.32	0.3	0.21
CaO	9.67	11.77	13.6	12.41	10.82	12.89	12.82	13.75
TiO_2	0.01	0.1	0.06	0.07	0.06	0.05		
FeO	0.36	0.53	0.61	0.54	0.56	0.45	0.66	0.58
Total	99.81	100.73	100.76	99.53	99.82	99.85	99.52	99.43
An	46.7	56.3	62.7	59.4	51.6	61.8	60.7	65.7
Al	53.3	43.7	37.3	40.6	48.4	38.2	39.3	34.3

Sample no	64.3.1 core	64.3.3 rim	64.3.4 pachy zone	64.3.5 microlite	64.1.1 core	64.1.2 pachy zone	64.1.4 rim	64.1.5 core	64.1.6 rim-1
SiO_2	58.04	52.65	51.73	56.12	57.04	50.72	51.2	56.53	52.26
TiO_2	0	0	0	0.18	0.03	0	0.02	0.01	0
Al_2O_3	25.58	28.52	29.52	27.32	26.25	30.23	29.29	26.17	29.52
FeO	0.3	0.58	0.55	0.85	0.43	0.4	0.58	0.41	0.4
CaO	8.51	12.47	13.43	11.13	9.25	14.36	13.55	9.49	13.56
Na_2O	6.31	4.55	4.17	4.97	6.21	3.59	4.04	6.07	4.15
K_2O	1.05	0.45	0.42	0.94	1.01	0.32	0.28	0.85	0.33
MgO	0	0.06	0	0	0	0.05	0.04	0.05	0
BaO	0.01	0.12	0.1	0.01	0.02	0.16	0.03	0.12	0.12
Total	99.8	99.4	99.92	101.52	100.24	99.83	99.03	99.7	100.34
An	42.7	60.2	64.0	55.3	45.1	68.8	64.9	46.3	64.3
Al	57.3	39.8	36.0	44.7	54.9	31.2	35.1	53.7	35.7

Sample no	64.1.7 rim-2	s64.1	s64.2	s64.4 core	s64.5 rim	s64.8 microlite
SiO_2	55.23	57.15	55.01	56.31	58.35	57.08
TiO_2	0	0	0.07	0.04	0	0
Al_2O_3	27.56	26.24	27.65	26.46	25.44	25.95
FeO	0.4	0.39	0.42	0.46	0.32	0.28
CaO	10.66	9.6	10.97	9.65	8.36	9.33
Na_2O	5.61	6.07	5.45	6.04	6.49	5.98
K_2O	0.6	0.83	0.49	0.81	1.19	0.76
MgO	0					
BaO	0.22					
Total	100.28	100.27	100.06	99.76	100.14	99.38
An	51.2	46.6	52.7	46.9	41.6	46.3
Al	48.8	53.4	47.3	53.1	58.4	53.7

Table 2. Continued.

Sample no	69.1.2 rim	69.1.1 core	69.2.2 core	69.2.3 rim	69.3.1 core	69.3.3 rim	69.3.2 microlite	74.2.3 core	74.2.1 rim	74.6.1 core	74.6.2 rim	74.8	74.4.1a
SiO_2	63.13	58.65	57.56	63.28	54.42	60.58	56.46	62.1	63.34	59.05	63.15	62.92	64.09
TiO_2	0	0	0	0.12	0.07	0	0	0	0.05	0	0	0	0.02
Al_2O_3	23.04	26.03	26.29	22.9	28.12	24.36	27.36	22.83	21.94	24.75	21.84	22.02	21.46
FeO	0.21	0.18	0.19	0.03	0.28	0.18	0.16	0.08	0.01	0.14	0.09	0.15	0.12
CaO	4.79	8.43	8.88	4.59	11.57	6.7	10.4	4.97	3.94	7.13	3.67	4.05	3.46
Na_2O	8.71	7.27	6.9	9.08	5.59	8.04	6.02	8.74	9.07	7.63	9	8.96	9.34
K_2O	0.95	0.42	0.37	0.84	0.29	0.57	0.39	0.68	0.87	0.41	0.99	0.92	0.86
MgO	0	0	0	0	0	0	0.01	0	0	0	0	0	0
BaO	0.11	0.17	0.21	0	0.03	0.27	0.11	0	0	0.03	0.11	0	0
Total	100.94	101.15	100.4	100.84	100.37	100.7	100.91	99.4	99.22	99.14	98.85	99.02	99.35
An	23.3	39.0	41.6	21.8	53.3	31.5	48.8	23.9	19.4	34.0	18.4	20.0	17.0
Al	76.7	61.0	58.4	78.2	46.7	68.5	51.2	76.1	80.6	66.0	81.6	80.0	83.0

Sample no	s29.4 core	s29.5 rim	s29p1 microlite	s29p2	s29p3	s29.3	23-pl	23-pl	23-pl0 microlite
SiO_2	53.85	56.05	54.48	57.73	54.02	59.41	57.42	60.07	54.03
TiO_2	0.12	0				0	0.00	0.05	0.12
Al_2O_3	28.56	26.9	28.31	25.47	27.67	25.15	25.94	24.42	28.64
FeO	0.33	0.39	0.56		0.46	0.15	0.14	0.21	0.62
CaO	11.93	10.08	11.73	8.42	11.34	7.54	9.10	6.94	12.26
Na_2O	5.16	6.01	5.12	6.91	5.38	7.61	6.11	6.98	4.60
K_2O	0.3	0.42	0.45	0.51	0.29	0.67	0.42	0.66	0.27
Total	100.24	99.85	100.65	99.03	99.14	100.53	99.13	99.38	100.53
An	56.1	48.1	55.9	40.2	53.8	35.4	45.2	35.5	59.6
Al	43.9	51.9	44.1	59.8	46.2	64.6	54.8	64.5	40.4

Sample no	s70.1 rim	s70.2 core	s70.8	s70.9 core	s70.11 rim1	s70.10 rim2	40-p4	40-pl
SiO_2	57.01	47.23	57.32	47.29	57.45	56.05	53.19	48.95
TiO_2	0	0.12	0.08	0.01	0.05	0.04	0.20	0.08
Al_2O_3	25.27	31.85	24.98	32.85	25.42	26.12	28.19	31.02
FeO	0.56	0.46	0.33	0.53	0.38	0.31	0.89	0.77
CaO	8.85	16.46	8.46	17.31	8.97	9.84	12.43	15.34
Na_2O	5.79	2.44	5.7	2.02	5.83	5.56	4.31	2.59
K_2O	1.39	0.08	1.74	0.06	1.36	1.06	0.22	0.13
Total	98.88	98.64	98.6	100.07	99.45	98.99	99.43	98.95
An	45.8	78.8	45.1	82.6	46.0	49.4	61.4	76.6
Al	54.2	21.2	54.9	17.4	54.0	50.6	38.6	23.4

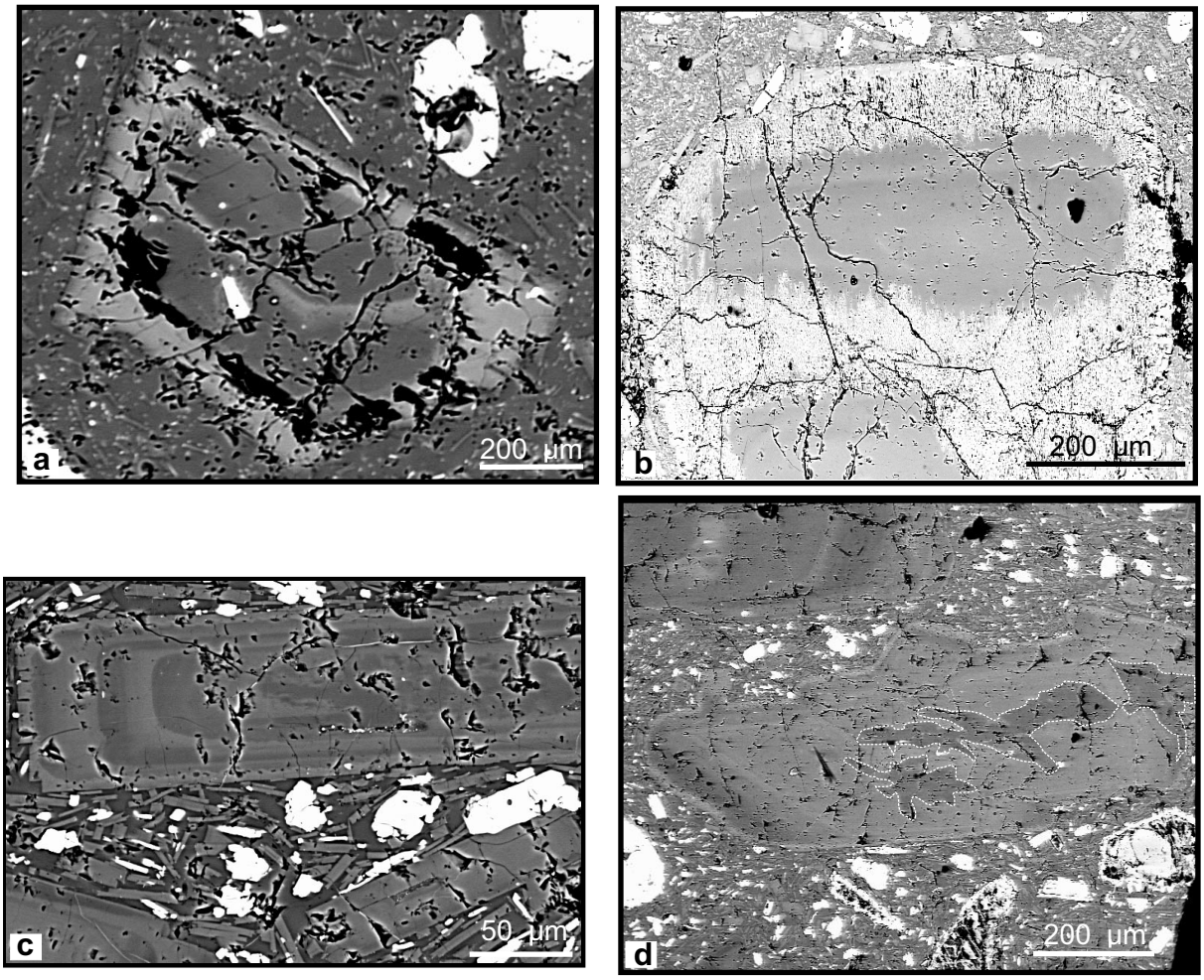

Figure 2. SEM images of plagioclase minerals. **(a)** Reversed zoned plagioclase phenocrysts with wide calcic rim and poorly developed sieve texture; **(b)** resorbed (fritted) texture of the plagioclase which has a dark sodic core and a light calcic rim; **(c)** oscillatory-zoned plagioclase; **(d)** patchy zoned plagioclase represents sieved textured areas.

oscillatory-zoned cores between An_{40} and An_{58} and rims typical between An_{60} and An_{68}. Many reversely zoned crystals remain calcic out to the edge of the grain but some have narrow more sodic rims; (iii) patchy-zoned crystals display anorthite-rich areas distributed in anorthite poor areas. Some phenocrysts have patchy zoning ranging up to about An_{69}.

In addition, sieve textures within an intimate network of calcic plagioclase and minute glass patches, commonly located near the outer part of the crystals occur sporadically.

Groundmass plagioclases in dacite samples, with An_{56-59}, are more calcic than the phenocrysts, but similar to those in andesites (An_{51-59}). Complex zoning, resorbed (fritted) textures, very common in acidic and andesitic samples, or rounded and/or mantled crystals indicate plagioclase-melt interactions as in the case of magma mixing. Resorbed or dusty plagioclase in the andesite is expected to form by changing physical conditions in a magmatic system, such as proposed for patchy zoning (cf. Stimac & Pearce 1992; Anderson 1984 and references therein).

Clinopyroxene (diopside) is the most common mafic phenocrysts of the Dikili group andesites and dacites and occurs as phenocrysts (0.4–1.5 mm) and micro-phenocrysts (0.2–0.4 mm) (Table 3). The former are

Table 3. Representative clinopyroxene analyses of the Dikili and Çandarlı lavas. Structural formulae of the clinopyroxenes on the basis of 6 oxygens.

Sample no	s70.1	s70.8	s70.28	s70.19	s70.11 core	s70.13.1 rim	s70.13.4 core	s70.13.9 rim	s70Qt1 quartz rim	s64.5 rim of opx	64.2.1 core	64.2.2 rim
Na_2O	0.39				0.49	0.54				0.47	0.25	0.19
MgO	15.24	18.03	16.74	18.4	16.79	14.09	17.24	13.99	16.07	14.01	15.49	18.43
Al_2O_3	3.27	1.07	1.2	0.81	2.75	2.78	1.18	1.4	0.54	1.97	2.97	0.98
SiO_2	50.86	53.6	52.15	53.33	50.97	50.92	52.24	50.84	52.99	51.51	50.92	53.23
CaO	22.41	21.33	19.84	21.72	21.98	20.63	21.65	21.36	20.64	21.73	22.46	21.7
TiO_2	0.69	0.39	0.29		0.35	0.72		0.53	0.43		0.41	0.31
Cr_2O_3	0.35		0.36	0.45	0.5		0.57				0.04	0.47
MnO		0.36							0.29	0.46	0.17	0.1
FeO	7.64	6.21	8.46	4.36	5.38	10.17	6.24	10.37	8.94	10.23	6.44	4.64
Total	100.84	100.99	99.04	99.08	99.23	99.86	99.12	98.49	100.49	100.36	99.15	100.05
Wo	45.21	41.62	39.90	42.83	44.38	42.83	42.87	43.67	41.31	44.17	45.81	42.59
En	42.76	48.93	46.82	50.46	47.15	40.69	47.48	39.78	44.73	39.61	43.94	50.31
Fs	12.03	9.46	13.28	6.71	8.48	16.48	9.64	16.55	13.96	16.23	10.25	7.11

Sample no	64.1.1 core	64.1.11 rim	64.1.2	83.p4	83.p6	83.p.13 core	83.p.14 rim	23-px1 horn. rim	23px2	s29.prx4	s29.prx5	s29prx1
Na_2O	0.33	0.51	0.45	0.37	0.28	0.4	0.18	0.40	0.39	0.33		
MgO	15.31	13.96	14.88	16.05	14.56	14.34	17.29	16.48	14.65	17.66	16.36	16.29
Al_2O_3	2.22	0.89	1.42	3.57	0.88	0.82	2.36	0.55	0.83	1.68	2.23	3.19
SiO_2	52.11	52.01	52.08	50.69	52.79	53.08	52.24	55.21	53.38	52.9	51.42	50.78
CaO	23.28	22.35	22.51	21.56	23.18	22.74	21.89	22.56	22.81	23	22.59	21.32
TiO_2	0.29	0.22	0.29	0.92	0.25	0.15	0.38	0.13	0.15	0.3	0.58	0.75
Cr_2O_3	0.28	0.08	0.09	0.26	0.03	0.15	0.3	0.06	0.00	0.6	0.31	
MnO	0.18	0.37	0.29	0.24	0.64	0.66	0.16	0.66	0.70			0.29
FeO	6.57	10.02	8.52	6.74	8.82	9.14	5.82	5.06	7.79	3.74	5.56	7.19
Total	100.57	100.41	100.53	100.4	101.43	101.48	100.62	101.12	100.68	100.2	99.05	99.81
Wo	46.84	45.07	45.15	43.87	46.07	45.65	43.36	45.63	46.30	45.56	45.47	42.99
En	42.84	39.16	41.51	45.42	40.25	40.04	47.64	46.38	41.36	48.66	45.80	45.69
Fs	10.32	15.77	13.34	10.70	13.68	14.32	9.00	7.99	12.34	5.78	8.73	11.32

Sample no	s12.1	s12.5	s12.6	83p1	83p8	s90.4	s90.5	s90.22
Na_2O				0.4	0.41	0.46		0.37
MgO	17.05	16.39	17.09	14.61	14.43	16.72	15.42	14.74
Al_2O_3	1.12	2.21	1.05	0.96	1.17	1.42		1.09
SiO_2	53.13	51.06	52.26	52.59	52.4	52.73	53.07	51.87
CaO	24.01	24.02	23.57	22.49	22.18	20.56	22.73	21.45
TiO_2	0.52	1.1	0.4			0.45		0.42
Cr_2O_3	0.49	0.27	0.69					
MnO				0.67	0.79	0.39		0.43
FeO	3.72	5.4	4.06	8.44	8.97	7.83	8.81	10.32
Total	100.04	100.45	99.11	100.16	100.35	100.06	100.03	100.69

Table 3. Continued.

Sample no	s12.1	s12.5	s12.6	83p1	83p8	s90.4	s90.5	s90.22
Wo	47.42	47.07	46.67	45.53	45.03	41.18	44.52	42.89
En	46.84	44.67	47.06	41.14	40.75	46.58	42.01	41.00
Fs	5.74	8.26	6.27	13.34	14.22	12.24	13.47	16.11

Sample no	11-px1	prx 5-11	40-px1 pachy zone	40-px2 pachy zone	40-px3 core	40-px4 rim
Na_2O	0.26	0.18	0.38	0.26	0.24	0.26
MgO	17.15	17.32	15.32	16.72	15.72	17.47
Al_2O_3	2.30	1.58	4.85	3.53	4.08	2.19
SiO_2	52.23	52.70	49.66	51.02	50.66	53.09
CaO	23.24	22.94	22.24	22.11	22.61	22.29
TiO_2	1.02	0.78	0.92	0.48	0.68	0.33
Cr_2O_3	0.69	0.11	0.33	0.90	0.43	0.53
MnO	0.10	0.14	0.25	0.05	0.04	0.16
FeO	4.39	5.25	5.79	4.79	5.66	4.98
Total	101.37	101.01	99.72	99.85	100.12	101.29
Wo	46.00	44.88	46.27	45.03	46.25	44.17
En	47.22	47.11	44.33	47.36	44.71	48.14
Fs	6.78	8.01	9.40	7.61	9.04	7.69

generally subhedral with patchy and oscillatory zoning, and commonly exhibit simple or lamellar twins (Figure 3). Zoned phenocrysts compositions vary between $Wo_{39–43}$ $En_{50–57}$ in core and $Wo_{39–47}$ $En_{41–51}$ in rim. Reaction rims of acicular augite and glass surrounding quartz xenocrysts are found in same lava types of the Dikili group.

Orthopyroxene is present as phenocryst and microphenocrysts in basaltic andesites and dacites (Table 4; Figure 4). Three phenocryst populations can be defined on the basis of their respective rim composition: (i) unzoned phenocrysts appear as two populations of En_{85} $Wo_{2–4}$ that are the most frequent or as En_{62}; (ii) normally ($Wo_{2.3}$ En_{78} in core, $Wo_{3.6}$ En_{66} in rim) and reversely ($Wo_{2.6}$ En_{74} in core, $Wo_{2.3}$ En_{85} in rim) zoned crystals; (iii) phenocrysts with overgrowths or reaction rims of augite or pigeonite have similar core compositions to the other unzoned phenocrysts.

There are also clinopyroxene (Wo_{40} En_{47} Fs_{12}) inclusions in the orthopyroxene (Wo_2 En_{66} Fs_{32}) crystals. Groundmass orthopyroxene are common and can be rimmed with pigeonite (Wo_{16} En_{54} Fs_{30}) or subcalcic augite.

Projected onto the temperature-contoured pyroxene quadrilateral (Lindsley 1983; Lindsley & Andersen 1983)

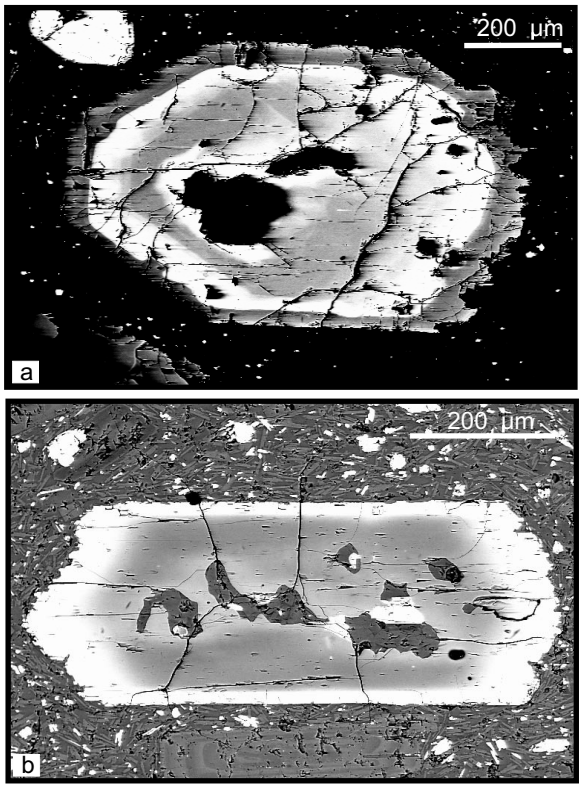

Figure 3. (a) Oscillatory zoning clinopyroxene crystals display two types of concentric bandings; (b) normal zoning clinopyroxene crystal have Mg-rich composition in large inner dark-coloured area.

Table 4. Representative orthopyroxene analyses of the Dikili and Çandarlı lavas. Structural formulae of the orthopyroxene on the basis of 6 oxygens.

Sample no	s70.2	s70.20	s64.2	s64.6	64.6.1	s90.6	s90.13 core	s90.14 rim	s90.16 core	s90.17 rim	s90.20	s90.24
Na_2O					0.05							
MgO	26.95	19.45	22.54	24.53	26.34	26.34	28.82	23.33	25.95	32.28	21.82	30.26
Al_2O_3	1.3	0.97	0.67	0.96	1.62	0.92	2.23	1.38	4.05	1.3	0.93	
SiO_2	53.04	45.91	52.14	52.49	52.83	53.99	53.92	51.96	51.37	55.51	51.69	55.5
CaO	1.17	7.77	1.03	1.15	1.23	1.43	1.21	1.79	1.28	1.24	1.3	1.15
TiO_2		0.32			0.18	0.3		0.35	0.51			
Cr_2O_3					0.15					0.64		0.51
MnO	0.51	0.62	0.73	0.58	0.39	0.46	0.27	0.49	0.5		0.61	
FeO	15.88	19.95	21.08	18.95	15.26	15.79	12.78	19.33	14.86	8.28	22.26	11.14
P_2O_5		4.97										
Total	98.85	99.95	98.2	98.65	98.05	99.23	99.25	98.63	98.77	99.27	98.61	98.55
Wo	2.29	15.42	2.11	2.30	2.47	2.84	2.36	3.63	2.61	2.36	2.65	2.21
En	73.43	53.68	64.20	68.16	73.60	72.70	78.18	65.78	73.70	85.36	61.91	81.04
Fs	24.28	30.90	33.69	29.55	23.93	24.46	19.46	30.59	23.68	12.29	35.44	16.74

Sample no	83.p8	s29.prx1 core	s29.prx2 rim	s29.prx3	s29prx3	40-px9
Na_2O	0.09					0.16
MgO	22.15	30.5	25.45	26.83	30.42	42.93
Al_2O_3	0.46	1.34	0.56	0.68	1.26	0.00
SiO_2	52.78	54.74	53.36	53.84	54.94	39.49
CaO	0.86	1.38	1.09	0.98	1.34	0.11
TiO_2	0.01				0.11	0.23
Cr_2O_3		0.39			0.39	0.03
MnO	1.43	0.3	0.71	0.64	0.21	0.28
FeO	21.88	10.5	17.85	16.29	10.11	18.09
P_2O_5						
Total	99.66	99.13	99.02	99.26	98.79	101.19
Wo	1.76	2.65	2.16	1.92	2.60	0.15
En	63.20	81.58	70.21	73.15	82.09	80.76
Fs	35.03	15.76	27.63	24.92	15.31	19.09

the pyroxene assemblages indicate temperatures of 900–1150 °C for andesite and 700–1100 °C for dacites (Figure 5). Previous studies indicate that the estimated pyroxene temperatures of the Middle Miocene lavas from the Dikili-Ayvalık-Bergama area vary between 820–1100 °C (Aldanmaz 2006).

Amphibole is a common phenocryst phase in the dacite and andesite, ranging between 0.5 mm and 1 cm in size (Table 5). It occurs as individual crystals and in clots with plagioclase, orthopyroxene and titanomagnetite. Fine-grained intergrowths of clinopyroxene, orthopyroxene, pigeonite, plagioclase and titanomagnetite occur as rims and along the cleavages of many crystals. In same cases, clinopyroxene forms an optically continuous patchwork texture replacing the original amphibole. This texture is believed to form

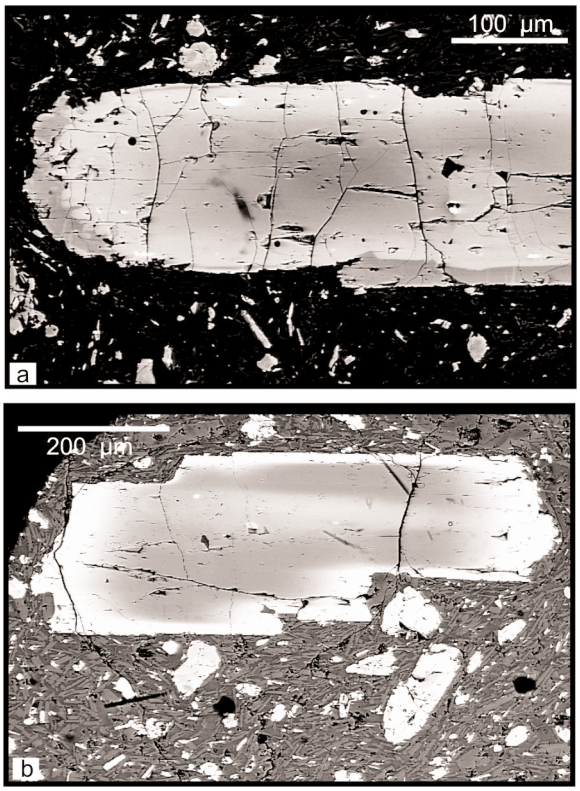

Figure 4. (a) Normal-zoned orthopyroxene with pigeonite (dark rim around the orthopyroxene); (b) normal-zoned resorbed orthopyroxene.

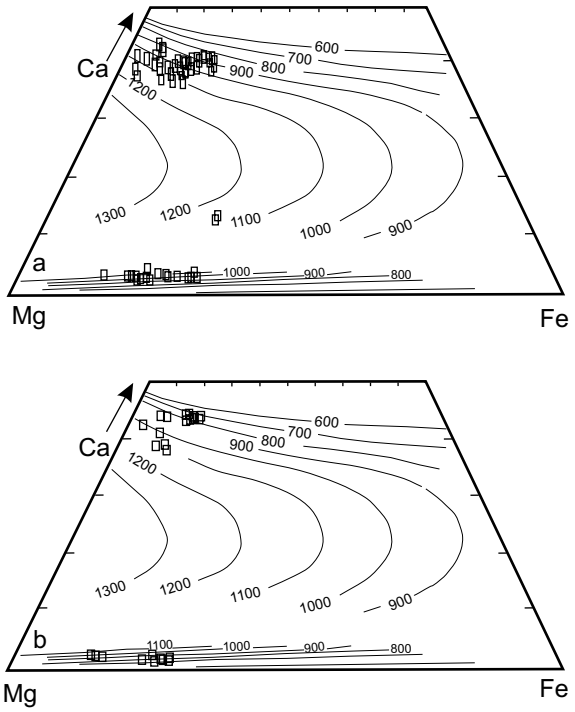

Figure 5. Pyroxene minerals compositions plotted on the pyroxene quadrilateral for (a) Dikili andesitic and (b) dacitic lavas. Tie-lines in the pyroxene quadrilateral join coexisting CPX and OPX phenocrysts at 5 kbar, based on the thermometry of Lindsley (1983). Ticks are in increments of 10%.

Table 5. Representative amphiboles analyses of the Dikili lavas. Structural formulae of the amphiboles on the basis of 23 oxygens.

Sample no	231	232	233	234	235	2318	29p1	2910	2917	29p5	29p12	291	298	2911	2912
SiO_2	47.39	47.51	48.76	46.7	46.05	40.53	44.57	46.58	45.04	44.18	44	43.67	43.21	41.18	44.41
Al_2O_3	7.68	7.53	6.49	8.09	7.7	11.57	9.08	6.68	8.23	9.23	9.03	9.03	9.12	11.28	9.51
TiO_2	1.52	1.42	1.24	1.72	1.31	2.54	2.39	1.35	1.37	2.34	2.53	1.98	2.68	3.58	2.79
FeO	13.53	13.5	13.72	14.2	14.25	16.21	13.35	13.24	14.54	13.46	13.78	16.11	11.82	10.85	12.25
MnO	0.48	0.5	0.49	0.29	0.51	0.41	0.41	0.43	0.42	0.31	0.38	0.52	0.26	0	0.29
MgO	14.45	14.42	15.03	13.88	13.32	10.71	13.89	14.65	13.43	14.11	13.62	12.19	13.99	13.91	14.65
CaO	11.79	11.93	11.83	11.94	11.7	12.18	12.06	11.96	12.39	12.14	12.08	12.31	12.1	12.13	11.89
Na_2O	1.47	1.19	1.19	1.37	1.17	1.81	1.86	1.4	1.57	1.91	1.9	1.78	1.89	2.07	2.1
K_2O	0.77	0.75	0.71	0.9	0.79	1.25	0.82	0.72	0.96	0.81	0.83	1.07	0.84	1	0.85
Total	99.08	98.75	99.46	99.09	96.8	97.21	98.43	97.01	97.95	98.49	98.15	98.66	95.91	96	98.74
Si	6.87	6.89	7.01	6.79	6.85	6.14	6.54	6.88	6.65	6.47	6.49	6.48	6.49	6.18	6.48
Al^{IV}	1.13	1.11	0.99	1.21	1.15	1.86	1.46	1.12	1.35	1.53	1.51	1.52	1.51	1.82	1.52
Al^{VI}	0.18	0.18	0.11	0.18	0.2	0.21	0.11	0.04	0.08	0.07	0.06	0.06	0.1	0.17	0.12
Ti	0.17	0.15	0.13	0.19	0.15	0.29	0.26	0.15	0.15	0.26	0.28	0.22	0.3	0.4	0.31
Fe^{3+}	0.06	0.15	0.15	0.1	0.17	0.3	0.14	0.24	0.33	0.25	0.18	0.3	0.09	0.05	0.04
Fe^{2+}	1.58	1.49	1.5	1.63	1.6	1.76	1.5	1.4	1.47	1.4	1.52	1.7	1.39	1.32	1.46
Mn^{2+}	0.06	0.06	0.06	0.04	0.06	0.05	0.05	0.05	0.05	0.04	0.05	0.07	0.03	0	0.04
Mg	3.12	3.12	3.22	3.01	2.95	2.42	3.04	3.23	2.96	3.08	3	2.7	3.13	3.11	3.19
Ca	1.83	1.85	1.82	1.86	1.86	1.98	1.9	1.89	1.96	1.91	1.91	1.96	1.95	1.95	1.86
Na	0.41	0.33	0.33	0.39	0.34	0.53	0.53	0.4	0.45	0.54	0.54	0.51	0.55	0.6	0.59
K	0.14	0.14	0.13	0.17	0.15	0.24	0.15	0.14	0.18	0.15	0.16	0.2	0.16	0.19	0.16

during ascent (cf. Devine *et al.* 1998) as amphibole becomes unstable at pressures less than 1.5 kbar and breaks down to form an anhydrous assemblage. Opaque replacement generally occurring at the rims and along cleavages may be complete in some slowly erupted samples through late-stage oxidation with the lava dome.

Amphibole analyses from the Dikili lavas are calculated with WinAmphcal-IMA-04 program (Yavuz 2007) and all samples are classified as calcic amphiboles. Magnesiohastingsite, edenit and magnesiohornblende are nearly same proportion, each group about one-third of all samples, based on the terminology of Leake *et al.* (1997) (Figure 6). Al_2O_3 contents are low, typically between 7 and 8%, extending up to 11% in a few crystals. These compositions are typical of amphiboles occurring in orogenic dacites and silisic andesites at continental margins (cf. Jakes & White 1972; Ewart 1979, 1982). The values of $(Na+K)_A$ are > 0.50 for high-K suite. Following Hammarstrom & Zen (1986), compositions derived from 70 amphibole samples indicate that estimated crystallization temperature and pressure values vary between 772–838 °C and 2.30–5.44 kb, respectively. In addition, Aldanmaz (2006) proposed 1095–820 °C temperatures for the Middle Miocene lavas of the Dikili-Ayvalık-Bergama area. On the other hand, the estimated pressures obtained from the hornblende geobarometer indicate two different ranges of crystallization pressures. The first one is 7.1–8.6 kbar and the other is 2.1–4.2 kbar, which suggest different levels crystallization depths for the Middle Miocene volcanic rocks.

Biotite forms subhedral to resorbed phenocrysts and microphenocrysts in andesites and dacites. Breakdown of biotite forms opaque oxides or a granular intergrowth of orthopyroxene, ilmenite, and magnetite. Apatite and Fe-Ti oxides occur as inclusions.

Quartz occurs typically as rounded individual crystals sometimes containing melt inclusions in the dacites. Quartz can also be found in the andesite but shows reaction rims of clinopyroxene and abundant interstitial glass (Figure 7a) at a short distance away from the edge of the quartz crystal.

Olivine can be identified as subhedral, small phenocrysts (Fo_{82-88}) in the basaltic andesites (Figure 7b, Table 6). Accessory minerals in Dikili group lavas include zircon and apatite.

Çandarlı Group

The rhyolites of Çandarlı group include lavas with felsitic, microlithic, granophyric or spherulitic types of groundmass, and glassy varieties. In their fine crystal groundmass, potassium feldspar (45%) and tridymite (up to 55%) are dominant; microlites of oligoclase, biotite and orthopyroxene also occur. Plagioclase phenocrysts are An_{17-20} in average; some display normal zoning between An_{24-34}–An_{20-17} rim. There are also quartz, biotite and amphibole; the content of the last two phases is up to 3–4%. Micro-phenocrysts of alkali feldspar (0.3–0.8%) are common.

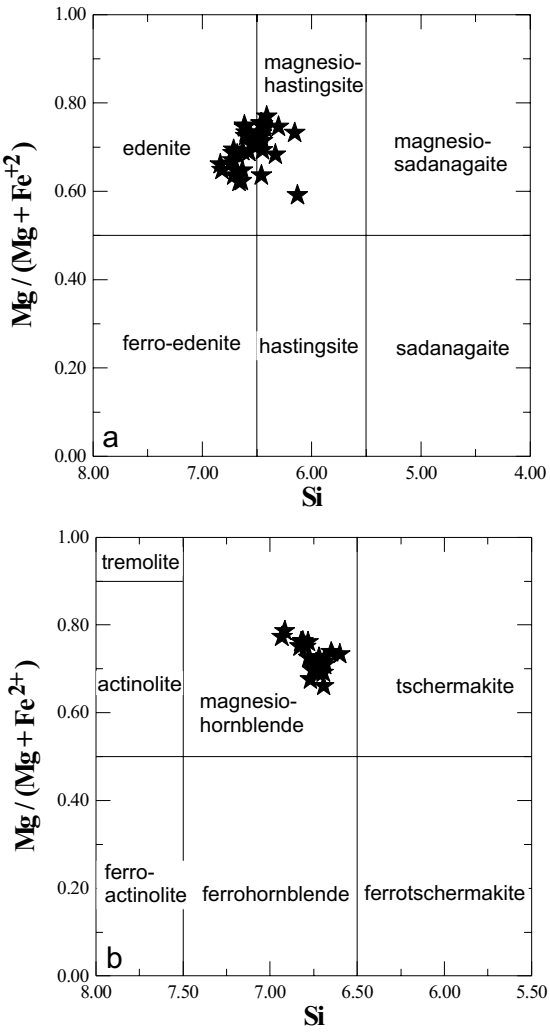

Figure 6. Amphibole minerals from Dikili lavas plotted on the classification diagram of Leake *et al.* (1997) on the basis of **(a)** (Na+K)≥ 0.50 and **(b)** (Na+K)≤ 0.50.

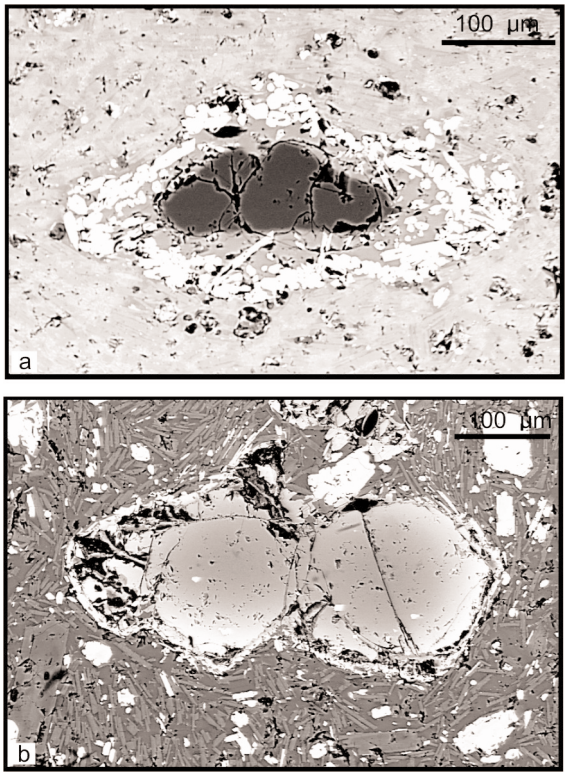

Figure 7. **(a)** Partially resorbed quartz phenocryst in basaltic andesite. The corona consists of bladed clinopyroxene with abundant interstitial glass; **(b)** resorbed- and normal-zoned olivine crystals in basaltic andesite, dark coloured areas indicates Mg-rich core.

Basaltic trachyandesite (BTA) is aphyric and contains only 5–10% phenocrysts of olivine, which are dominated by euhedral Mg-rich (Fo_{90}) and show a slightly normal zonation (Table 6). Small micro-phenocrysts of clinopyroxene are euhedral, Ca-rich ($Wo_{44–46}$) with 0.3–0.9% Cr_2O_3, and mainly diopsite-salite in composition. Zoning is highly variable, either normal or inverse.

Clinopyroxene, plagioclase ± olivine are the common phenocrystals in basaltic andesites. Most of the olivine phenocrysts exhibit normal compositional zoning with more Mg-rich cores ($Fo_{82–87}$) and Fe-rich mantles ($Fo_{77–82}$).

Plagioclase and clinopyroxene form small phenocrysts. Average composition of plagioclase is $An_{61–77}$ and one sample displays very high anorthite content of An_{80} (core) and An_{85} (rim). Composition of clinopyroxene varies between $Wo_{44–46}$ $En_{44–48}$.

Basaltic andesite contains oval or blocky holocrystalline quartz-dioritic to tonalitic enclaves (diameter 15–2 cm).

Whole Rock Chemistry

Major and trace element compositions (Table 7) of all the Dikili-Çandarlı samples show a wide range of SiO_2 contents ranging between 51% and 80% and exhibit a complete compositional series from basaltic andesite to rhyolite. All the samples classify as sub-alkaline with respect to the Irvine & Baragar (1971) subdivisions (Figure 8), with the exception of the Çandarlı BTA, which is alkaline. Dikili group plots on the boundary line between trachyandesite-trachydacite and andesite-dacite fields in Figure 8. However, Çandarlı group is bimodal with basaltic trachyandesite (BTA)/basaltic andesites on one hand and rhyolites on the other hand. In a plot of K_2O versus SiO_2 (Figure 9), the samples plot predominantly within the high-K field again BTA is displaced to higher potassium. General pattern of Dikili and Çandarlı groups is similar to many high-K, calc–alkaline volcanic series from Aegean region volcanic rocks and also active continental margins (Wilson 1989 and references therein; Yılmaz *et al*. 2001 and references therein).

Selected major element oxides for both series are plotted against SiO_2 content in Figure 10. In the Harker diagrams, as SiO_2 increases TiO_2, CaO, MgO decrease and K_2O increases (Figures 9 & 10). Such linear trends as negative and/or positive correlations can be explained by fractional crystallization. The Al_2O_3-SiO_2 diagram shows that plagioclase is an important fractionating phase from 60% SiO_2 on Figure 10. There is a major inflection in Na_2O at about 70% SiO_2 that indicates plagioclase and/or anorthoclase fractionation (Figure 10) (Cox *et al.* 1979 and references therein). Decrease in CaO is consistent with fractionation of plagioclases and clinopyroxene. Decreasing MgO and Fe_2O_3 is related to olivine, pyroxene and possibly Fe-Ti oxides fractionation (Figure 10)

Selected trace element variation diagrams are plotted in Figure 11. There is no noticeable linear trend in these diagrams. There is slight enrichment in Rb, Nb with increasing silica while Zr and Sr represent slightly negative trends. There are various inflections in the patterns caused by sudden decreases in trace element concentrations in boundary between Dikili and Çandarlı lavas. Lavas display major inflections in Sr, Zr and Ba at

Table 6. Representative microprobe analyses of olivine phenocrysts (pc) and microphenocrysts (mic pc) of Dikili and Çandarlı lavas.

Sample no	11.2	11.4	11.5	11.6	11.7.3	11.7.6	11.7.8	11.8.1	11.8.6	40.2	40.3	40.7	40.9	40.5	40.6	90.2	90.5	90.7
	unhedral	unhedral	matrix	matrix	micro pc	micro pc	micro pc	pc.	pc.					core	rim	rim	pc.	pc.
SiO_2	40.36	41.34	40.28	39.43	40.37	40.00	39.04	41.15	38.05	40.09	38.98	38.13	39.53	39.11	38.36	38.82	39.15	40.14
NiO	0.41	0.51	0.58					0.43										
FeO	10.82	7.17	11.55	16.13	10.76	13.88	17.20	8.74	18.62	12.56	20.26	23.43	14.35	16.71	20.68	16.91	14.12	11.51
MnO									0.35	0.24	0.39	0.65	0.31	0.31	0.39	0.34	0.32	0.00
MgO	48.22	51.26	47.76	43.52	47.95	46.63	43.50	50.35	39.56	46.60	40.85	37.12	45.13	42.87	39.78	43.40	45.30	48.02
CaO			0.19		0.34	0.30				0.15	0.24	0.13	0.15	0.21	0.15			
Total	99.80	100.28	100.36	99.08	99.42	100.81	100.17	100.67	96.59	99.67	100.75	99.51	99.48	99.21	99.39	99.47	98.90	99.67
Formulas on the basis of 4 oxygens																		
Si	0.997	0.999	0.994	1.003	0.999	0.991	0.993	0.998	1.008	0.999	0.997	1.004	0.996	0.999	0.998	0.991	0.992	0.994
Ni	0.008	0.010	0.012	0.000	0.000	0.000	0.000	0.008	0.000	0.000	0.000	0.000	0.000	0.000	0.000	0.000	0.000	0.000
Fe	0.223	0.145	0.238	0.343	0.223	0.288	0.366	0.177	0.413	0.262	0.433	0.516	0.302	0.357	0.450	0.361	0.299	0.238
Mn	0.000	0.000	0.000	0.000	0.000	0.000	0.000	0.000	0.008	0.005	0.008	0.015	0.007	0.007	0.009	0.007	0.007	0.000
Mg	1.775	1.847	1.757	1.650	1.769	1.722	1.649	1.819	1.563	1.731	1.557	1.457	1.695	1.632	1.542	1.651	1.710	1.773
Ca	0.000	0.000	0.005	0.000	0.009	0.008	0.000	0.000	0.000	0.004	0.007	0.004	0.004	0.006	0.004	0.000	0.000	0.000
Total	3.003	3.001	3.006	2.997	3.001	3.009	3.007	3.002	2.992	3.001	3.003	2.996	3.004	3.001	3.002	3.009	3.008	3.006
Fo	0.89	0.93	0.88	0.83	0.89	0.86	0.82	0.91	0.79	0.87	0.78	0.74	0.85	0.82	0.77	0.82	0.85	0.88
Fa	0.11	0.07	0.12	0.17	0.11	0.14	0.18	0.09	0.21	0.13	0.22	0.26	0.15	0.18	0.23	0.18	0.15	0.12

Table 7. Major (wt%) and trace element (ppm) analyses of the Dikili and Çandarlı lavas. bta: basaltic trachyandesite, ba: basaltic andesite, rhy: rhyolite (Sample EA350 taken from Aldanmaz *et al.* 2000).

Sample no	EA350	ZK-11	ZK-71	ZK-D40	ZK-70	ZK-90	ZK-47
Group	Çandarlı (bta)	Çandarlı (bta)	Çandarlı (bta)	Çandarlı (bta)	Çandarlı (bta)	Dikili	Dikili
SiO_2 (wt%)	51.24	51.44	52.90	53.55	57.06	60.89	61.88
TiO_2	1.22	1.18	0.77	0.75	0.78	0.61	0.52
Al_2O_3	11.69	11.04	14.20	14.44	13.97	14.60	15.91
Fe_2O_3	7.51	7.25	7.46	7.34	5.56	5.85	4.02
MgO	12.62	12.70	9.64	9.77	4.25	4.50	2.59
MnO	0.12	0.11	0.12	0.12	0.15	0.10	0.08
CaO	7.58	7.59	8.87	8.79	7.84	6.47	4.79
K_2O	4.72	4.05	1.85	1.83	2.90	2.58	3.34
Na_2O	1.7	1.66	2.64	2.73	2.52	3.03	2.91
P_2O_5	0.67	0.60	0.23	0.24	0.35	0.18	0.17
LOI	2.54	2.99	1.24	1.18	2.26	1.54	2.44
Total	101.61	100.61	99.92	100.75	97.64	100.35	98.65
Sc	14.03	26.0	26.3	28.3	23.6	17.6	13.0
V	169.9	185.4	175.3	182.3	164.0	157.2	104.0
Cr	755	864.4	484.0	499.6	199.3	142.0	57.0
Co	31.9	45.5	35.2	36.8	25.9	20.8	12.3
Ni	456.8	443.8	225.0	257.7	68.2	55.0	17.0
Cu	42.3	62.8	56.1	153.2	33.8	29.0	22.0
Zn	55.7	70.7	60.5	69.9	69.6	61.1	59.4
Rb	173.8	125.6	70.0	63.0	168.7	86.3	137.1
Sr	713.4	693.5	773.7	759.9	574.0	772.5	621.5
Y	21.7	21.9	22.4	22.5	23.8	23.2	24.0
Zr	408.5	221.2	135.2	131.3	211.5	135.2	0.0
Nb	30	33.63	8.823	8.827	16.5	9.1	12.0
Cs	6.2	5.6	2.0	1.8	8.6	3.1	4.9
Ba	917.9	986.0	1073.0	1178.0	1107.0	1603.0	1461.0
La	43.75	46.09	33.43	33.29	38.79	32.69	56.24
Ce	107.2	103.40	63.53	62.03	73.36	60.05	89.11
Pr	13.99	12.90	7.53	6.53	7.99	6.86	9.15
Nd	60.45	58.44	28.30	27.93	34.41	24.97	35.47
Sm	9.57	9.47	5.22	5.17	6.08	4.69	5.96
Eu	1.97	2.00	1.47	1.39	1.40	1.47	1.41
Gd	6.04	6.55	4.66	4.53	4.92	4.46	5.08
Tb	0.83	0.78	0.66	0.62	0.67	0.65	0.67
Dy	4.07	3.96	3.64	3.65	3.79	3.68	3.84
Ho	0.73	0.71	0.72	0.72	0.74	0.74	0.74
Er	1.77	1.93	2.03	2.07	2.13	2.10	2.12
Tm	0.3	0.27	0.26	0.31	0.32	0.28	0.32
Yb	1.65	1.66	2.00	1.96	2.03	2.12	2.07
Lu	0.26	0.26	0.31	0.31	0.33	0.33	0.33
Hf	10.62	11.17	3.42	3.43	5.96	3.68	2.18
Ta	1.87	1.85	0.55	0.51	1.08	0.61	0.98
Pb	22.08	16.79	33.18	28.12	27.78	48.64	41.16
Th	29.3	27.74	12.38	11.26	25.17	12.04	23.08
U	7.01	7.79	2.45	2.70	7.40	3.03	6.69

Table 7. Continued.

Sample no Group	ZK-D21 Dikili	ZK-D15 Dikili	ZK-64 Dikili	ZK-22 Dikili	ZK-81 Dikili	ZK-83 Dikili	ZK-D23 Dikili
SiO_2 (wt%)	62.14	62.33	62.40	62.63	63.58	63.71	64.22
TiO_2	0.69	0.70	0.62	0.67	0.66	0.64	0.59
Al_2O_3	14.81	15.55	15.18	15.19	14.98	14.09	14.46
Fe_2O_3	5.67	5.54	5.08	5.29	5.11	5.11	4.41
MgO	3.39	2.64	2.70	3.12	2.38	3.09	2.21
MnO	0.10	0.10	0.06	0.10	0.08	0.09	0.08
CaO	5.75	5.69	5.78	5.77	5.55	5.47	4.59
K_2O	3.72	2.86	3.00	3.37	3.48	3.52	3.41
Na_2O	3.14	3.52	3.22	3.33	3.60	3.48	3.06
P_2O_5	0.28	0.25	0.25	0.28	0.29	0.27	0.25
LOI	1.10	1.30	2.58	1.24	1.14	1.29	2.07
Total	100.78	100.48	100.88	100.99	100.86	100.61	99.35
Sc	15.3	15.3	15.9	14.3	14.1	12.7	3.4
V	126.8	113.9	115.3	120.1	126.2	109.7	2.1
Cr	137.3	134.6	130.0	125.7	80.7	97.3	36.3
Co	18.7	18.6	14.4	18.8	15.1	15.3	0.8
Ni	58.8	178.0	51.0	78.7	34.0	54.5	16.2
Cu	25.9	32.8	11.6	28.0	22.2	18.8	3.4
Zn	60.0	60.7	55.9	64.0	58.8	58.3	87.7
Rb	140.3	127.4	166.6	138.4	142.7	142.1	80.0
Sr	577.6	582.3	625.2	595.5	577.7	580.5	340.6
Y	21.6	21.9	21.9	21.1	22.7	22.6	16.1
Zr	271.9	206.1	187.0	187.8	199.7	202.7	186.8
Nb	16.4	15.7	14.2	15.8	16.7	16.7	20.1
Cs	5.0	3.5	7.1	5.0	4.2	4.9	5.1
Ba	1110.0	1105.0	1026.0	1100.0	1113.0	1085.0	1258.0
La	45.03	43.68	41.90	44.55	46.63	46.49	46.71
Ce	73.07	73.07	71.79	72.04	72.07	72.34	78.90
Pr	7.81	7.42	7.92	7.55	7.80	7.70	7.81
Nd	31.02	29.50	32.21	30.01	30.85	30.28	26.47
Sm	5.24	4.99	5.50	5.03	5.14	5.00	4.26
Eu	1.32	1.30	1.30	1.33	1.31	1.28	1.04
Gd	4.46	4.37	4.59	4.30	4.43	4.31	3.48
Tb	0.60	0.59	0.61	0.58	0.61	0.58	0.45
Dy	3.44	3.43	3.51	3.29	3.54	3.43	2.64
Ho	0.66	0.68	0.68	0.65	0.70	0.68	0.49
Er	1.93	1.96	1.94	1.88	2.05	2.01	1.29
Tm	0.29	0.30	0.29	0.28	0.32	0.31	0.18
Yb	1.92	1.91	1.82	1.85	2.05	2.01	1.33
Lu	0.31	0.31	0.29	0.30	0.34	0.33	0.20
Hf	3.68	3.69	4.36	3.37	3.37	3.74	3.11
Ta	1.15	1.12	1.09	1.13	1.22	1.21	1.61
Pb	25.45	26.44	33.59	26.20	27.18	26.79	53.24
Th	19.97	19.28	21.89	19.79	21.62	21.50	28.36
U	5.52	5.03	6.56	5.48	5.77	5.91	2.44

Table 7. Continued.

Sample no	ZK-D18	ZK-29	ZK-42	ZK-10	ZK-34	ZK-1	ZK-46
Group	Dikili	Dikili	Dikili	Dikili	Dikili	Dikili	Dikili
SiO_2 (wt%)	64.53	64.68	65.47	66.21	68.06	70.39	70.97
TiO_2	0.52	0.65	0.51	0.34	0.64	0.43	0.36
Al_2O_3	14.75	15.42	14.61	14.11	12.23	13.81	14.07
Fe_2O_3	4.29	4.37	3.76	3.02	4.99	3.44	3.34
MgO	2.37	2.35	2.09	1.29	2.29	1.25	1.07
MnO	0.10	0.08	0.07	0.06	0.06	0.04	0.04
CaO	5.33	4.55	4.42	3.45	5.22	3.55	3.26
K_2O	3.58	3.72	4.14	3.34	3.55	3.29	3.82
Na_2O	3.24	3.56	3.23	3.57	2.83	3.45	3.59
P_2O_5	0.18	0.29	0.24	0.13	0.41	0.16	0.15
LOI	2.24	1.92	2.31	2.65	1.14	1.11	0.62
Total	101.14	101.59	100.85	98.18	101.42	100.92	101.28
Sc	12.8	10.2	10.4	7.9	15.9	9.2	8.8
V	97.7	82.1	86.6	59.4	83.0	80.4	61.4
Cr	76.2	51.5	41.9	30.5	166.1	24.2	21.8
Co	15.3	12.7	10.7	8.6	14.7	8.5	7.3
Ni	54.9	29.8	21.5	13.8	32.6	3.9	4.6
Cu	25.2	7.9	8.2	6.9	18.0	5.9	12.2
Zn	55.4	62.2	52.6	45.6	46.3	40.7	44.3
Rb	172.7	158.0	151.1	158.6	142.3	118.2	157.2
Sr	440.3	505.4	558.2	512.4	526.3	503.0	471.9
Y	21.5	25.5	19.1	18.4	19.7	22.3	16.7
Zr	199.4	275.9	169.8	150.6	190.6	179.7	135.4
Nb	13.7	20.0	15.9	12.0	13.4	11.2	11.8
Cs	7.2	6.8	5.6	6.9	4.6	3.9	3.2
Ba	886.9	999.4	1392.0	1216.0	1284.0	1362.0	1166.0
La	38.74	46.45	42.53	49.07	35.45	47.69	48.61
Ce	69.89	74.01	71.05	76.26	62.73	75.78	74.29
Pr	6.90	8.26	6.86	7.52	6.63	7.97	7.63
Nd	27.30	33.01	26.60	28.23	27.86	31.16	28.68
Sm	4.73	5.57	4.40	4.54	4.84	5.23	4.66
Eu	1.07	1.35	1.16	1.08	1.25	1.18	1.08
Gd	4.06	4.80	3.77	3.77	4.12	4.50	3.83
Tb	0.57	0.67	0.51	0.50	0.55	0.61	0.50
Dy	3.34	3.91	2.99	2.86	3.11	3.49	2.76
Ho	0.65	0.78	0.58	0.55	0.60	0.67	0.52
Er	1.94	2.28	1.70	1.59	1.75	1.94	1.46
Tm	0.30	0.35	0.26	0.24	0.26	0.29	0.22
Yb	1.94	2.29	1.68	1.60	1.66	1.87	1.42
Lu	0.31	0.37	0.27	0.25	0.26	0.29	0.22
Hf	5.09	5.47	2.31	2.09	3.63	1.87	2.15
Ta	1.13	1.45	1.25	1.03	0.91	0.91	1.01
Pb	32.81	25.50	30.86	44.84	22.57	39.22	44.86
Th	23.51	21.21	21.54	25.50	16.44	21.35	25.19
U	7.52	6.75	6.52	6.70	3.43	3.74	5.04

Table 7. Continued.

Sample no	ZK55	ZK-D3	ZK-23	ZK66	ZK69A	ZK74	ZK61A	ZK62B
Group	Çandarlı (rhy)	Çandarlı (rhy)	Çandarlı (rhy)	Çandarlı (rhy)	Çandarlı (rhy)	Çandarlı (rhy)	Çandarlı (rhy)	Çandarlı (rhy)
SiO_2 (wt%)	71.22	71.48	72.92	73.29	74.01	75.12	76.21	80.98
TiO_2	0.16	0.14	0.16	0.15	0.09	0.08	0.09	0.09
Al_2O_3	13.38	13.26	14.73	13.07	12.70	12.10	12.99	11.37
Fe_2O_3	1.49	1.28	1.10	1.38	0.67	0.64	0.40	0.51
MgO	0.34	0.29	0.51	0.42	0.23	0.16	0.16	0.24
MnO	0.07	0.07	0.02	0.06	0.05	0.07	0.02	0.01
CaO	1.68	1.47	2.01	1.72	1.70	0.85	0.51	0.47
K_2O	3.52	4.54	3.86	3.84	3.65	4.01	4.54	3.57
Na_2O	3.81	3.69	3.76	3.27	3.12	2.71	2.33	1.43
P_2O_5	0.07	0.06	0.08	0.07	0.04	0.04	0.05	0.04
LOI	3.04	3.51	2.39	2.85	4.65	3.14	2.42	3.06
Total	98.77	99.79	101.53	100.13	100.90	98.92	99.72	101.76
Sc	4.7	4.1	11.4	4.7	3.2	5.5	4.1	3.5
V	4.3	3.3	104.3	9.3	1.3	1.2	5.6	3.6
Cr	9.1	6.6	8.8	8.3	11.6	7.7	9.0	15.2
Co	1.4	0.6	13.3	1.7	0.7	0.8	0.9	1.2
Ni	1.1	14.3	28.6	13.6	4.6	1.6	11.6	33.6
Cu	4.1	-1.5	15.1	4.9	2.8	4.1	7.6	5.1
Zn	85.5	37.3	56.8	77.0	22.9	81.8	61.2	68.8
Rb	167.6	184.1	161.4	191.5	236.8	227.2	195.7	189.1
Sr	246.4	204.8	545.5	225.2	280.9	25.4	84.1	70.8
Y	20.2	19.8	20.8	23.5	20.9	25.6	13.6	13.7
Zr	162.2	142.6	189.4	126.2	69.3	51.6	69.2	69.2
Nb	18.0	19.0	16.4	21.1	23.1	24.1	22.9	17.9
Cs	8.2	9.0	8.4	8.5	183.3	10.0	6.7	9.5
Ba	1114.0	1071.0	1190.0	681.2	993.0	139.4	551.8	851.2
La	49.20	43.83	45.71	28.28	24.28	18.13	26.33	22.73
Ce	81.02	72.51	74.13	48.89	45.85	35.28	46.72	38.93
Pr	8.04	6.66	7.60	5.40	4.84	3.77	5.21	4.15
Nd	26.95	23.93	29.68	19.50	16.87	12.93	17.86	13.92
Sm	4.38	3.93	4.95	3.96	3.55	3.20	3.49	2.45
Eu	0.90	0.76	1.23	0.70	0.65	0.27	0.54	0.54
Gd	3.64	3.31	4.18	3.49	3.15	3.03	2.73	2.03
Tb	0.49	0.48	0.57	0.53	0.47	0.51	0.37	0.29
Dy	3.04	2.91	3.32	3.45	3.06	3.55	2.18	1.99
Ho	0.61	0.57	0.64	0.70	0.62	0.74	0.41	0.42
Er	1.71	1.70	1.87	1.94	1.72	2.11	1.13	1.21
Tm	0.26	0.27	0.29	0.30	0.26	0.33	0.17	0.20
Yb	2.04	1.83	1.84	2.31	2.03	2.61	1.28	1.60
Lu	0.32	0.29	0.29	0.36	0.31	0.40	0.20	0.24
Hf	3.73	3.07	2.91	2.66	2.53	2.20	2.71	2.97
Ta	1.55	1.65	1.27	1.77	1.86	2.25	1.99	1.80
Pb	62.77	50.58	30.09	68.36	64.96	74.27	68.15	54.18
Th	28.35	27.73	21.32	26.09	26.76	22.93	24.11	21.90
U	6.93	8.78	6.39	7.73	7.31	10.16	5.20	5.08

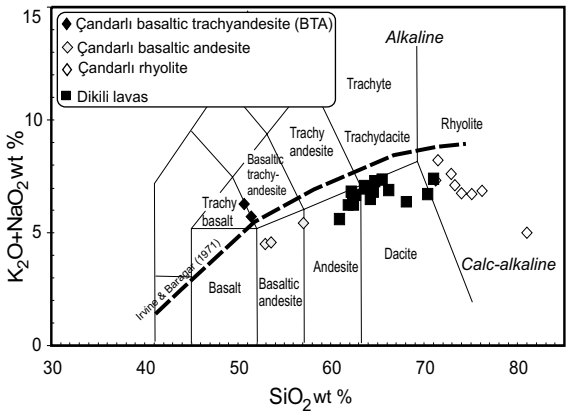

Figure 8. The classification of components of the Dikili-Çandarlı lavas. The diagram style is after Le Maitre (1989).

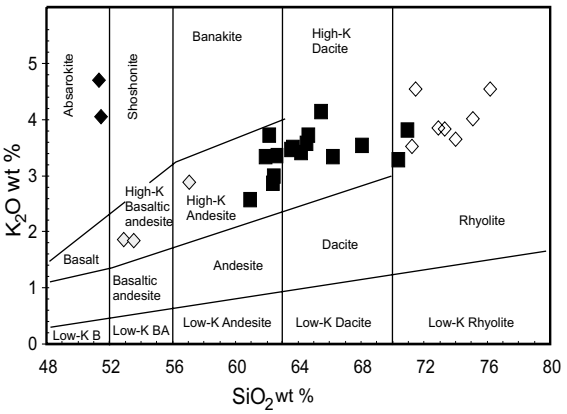

Figure 9. K_2O vs SiO_2 plot for magmatic rocks (after Le Maitre 1989). Symbols are same as Figure 8.

about 70% SiO_2 that can clearly be attributed to alkali feldspar as a crystallizing phase (Cox *et al.* 1979 and references therein). Ni represents negative correlation with an increase in silica content. However, some samples of the Dikili lavas have high Ni concentration at particularly high silica contents, such as 79–178 ppm Ni at 62% SiO_2. These trace element characteristics of Dikili Çandarlı lavas seem to indicate that besides magmatic differentiation more complex processes, such as magma mixing and crustal contamination may have played a role.

Two samples (EA350 and ZK-11) represent the basaltic trachyandesite (BTA) dykes of the Çandarlı group (Table 7). Mineralogical and chemical composition of the BTA is very different from the other lavas in the region which is ultrapotassic rock (MgO> 3 wt%, K_2O> 3 wt%, K_2O/Na_2O> 2) according to the classification by Foley *et al.* (1987). BTA is alkaline and TiO_2, K_2O and MgO values are richer than the other lavas. Its high MgO (12%), Ni (444 ppm), and Cr (864 ppm), low FeO/MgO ratio (0.51) and Al_2O_3 content (11 %) correspond to quite primitive characteristic. Main mineralogical features of the BTA dykes are Mg-rich olivine and pyroxene phenocryst (Tables 3 & 6). All these features indicate that olivine crystals are not inherited xenocrysts, but true magmatic phenocrysts in equilibrium with the host basaltic melt (cf. Simkin & Smith 1970; Nye & Reid 1986). Such Mg-rich basaltic rocks not commonly occur in the Aegean volcanic rocks. Çandarlı alkaline BTA represents similar geochemical features with Tertiary ultrapotassic alkaline volcanism, which has been reported in a few localities of western Anatolia, such as Bodrum (Robert *et al.* 1992), Uşak-Selendi-Emet regions (Seyitoğlu *et al.* 1997) and Afyon region on west-central Anatolia (Keller 1983; Savaşçın *et al.* 1995; Francalanci *et al.* 2000; Akay 2003; Aydar *et al.* 2003).

Petrogenetic Modelling

Petrographic and geochemical features suggest that the magma mixing process may have been affective in the generation of the Dikili lavas; for these reason diagrams in Figure 12 have been drawn to understand the role of magma mixing in the evolution of the Dikili lavas. In these diagrams, incompatible elements (Rb, Th) were plotted against compatible elements (Sc, Co) to provide a comparison with the theoretical fractional crystallization curve (Figure 12). Rayleigh equation was used to obtain the fractional crystallization (FC) curve and the most primitive sample (ZK–D40) was used as an initial composition. Tick marks on the FC curves correspond to 10% crystallization intervals. The calculation was made for 50% plagioclase + 30% amphibole + 15% clinopyroxene + 5% orthopyroxene compositions typical for intermediate lavas. Distribution coefficient (Kd) values are calculated as Kd_{Rb}= 0.043, Kd_{Th}= 0.075, Kd_{Co}= 4.65 and Kd_{Sc}= 3.6 for these composition because this combination gives best fit for fractional crystallization (FC) curve (Kd values of the minerals taken from Rollinson 1993). In addition to FC line, two different groups of lines are also plotted in these diagrams. The first group represents possible mixing lines between the primitive and more evolved samples. Most of the samples

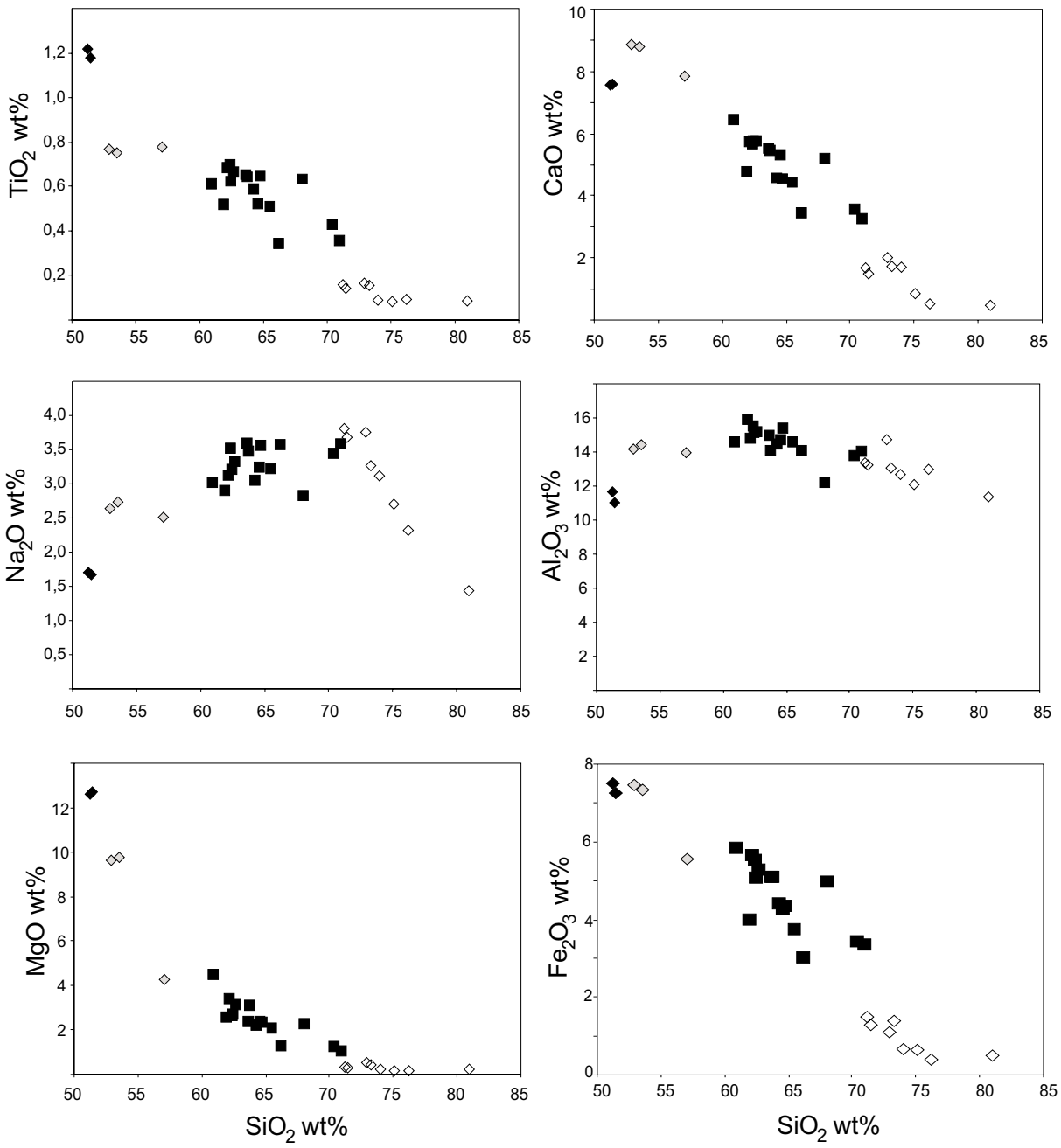

Figure 10. Variation diagrams of selected major elements versus silica. Symbols are same as Figure 8.

are plotted on the possible mixing lines rather than FC line in these diagrams (Figure 12). The second group lines are calculated, based on decreasing Kd_{Co} and Kd_{Sc} at constant Kd_{Rb} and Kd_{Th} values, and four different FC curves are obtained and we found that most of the Dikili samples plotted on these calculated curves. Because mineral distribution coefficients do not change within the closed magma chamber, this indicates that the system was not closed and magma mixing processes may have occurred.

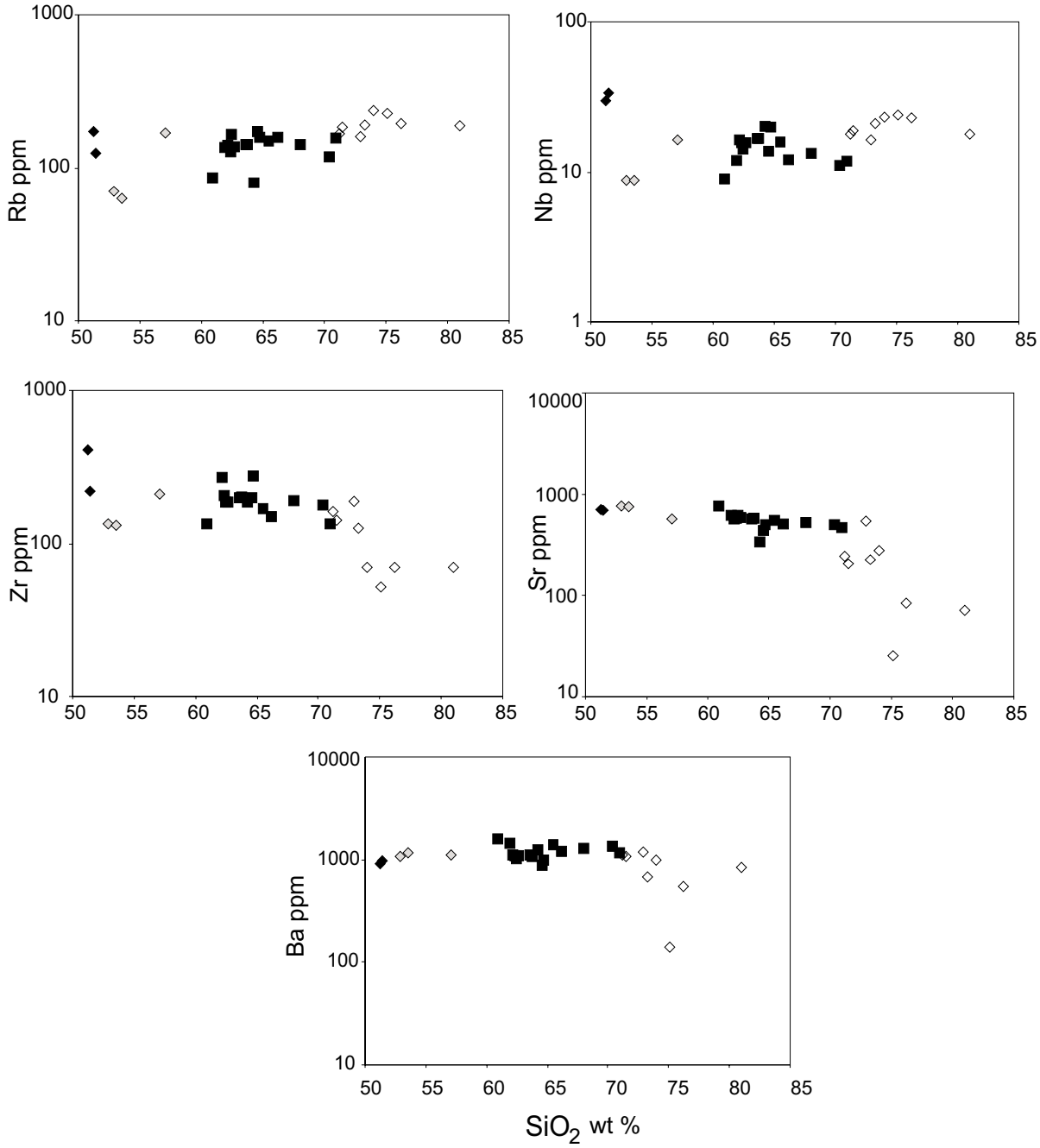

Figure 11. Variation diagrams of selected trace elements versus silica. Symbols are same as Figure 8.

Rare-Earth Element Patterns

The chondrite-normalized rare-earth element (REE) patterns of the Dikili lavas display sub-parallel trends with nearly constant concentration ratios (Figure 13). Regarding the Çandarlı volcanics, the BTA mafic lavas are the most LREE enriched and show a different pattern. Other mafic (basaltic andesites) and felsic lavas of the Çandarlı group represent very similar trend with the Dikili group. However, felsic lavas are depleted and show a

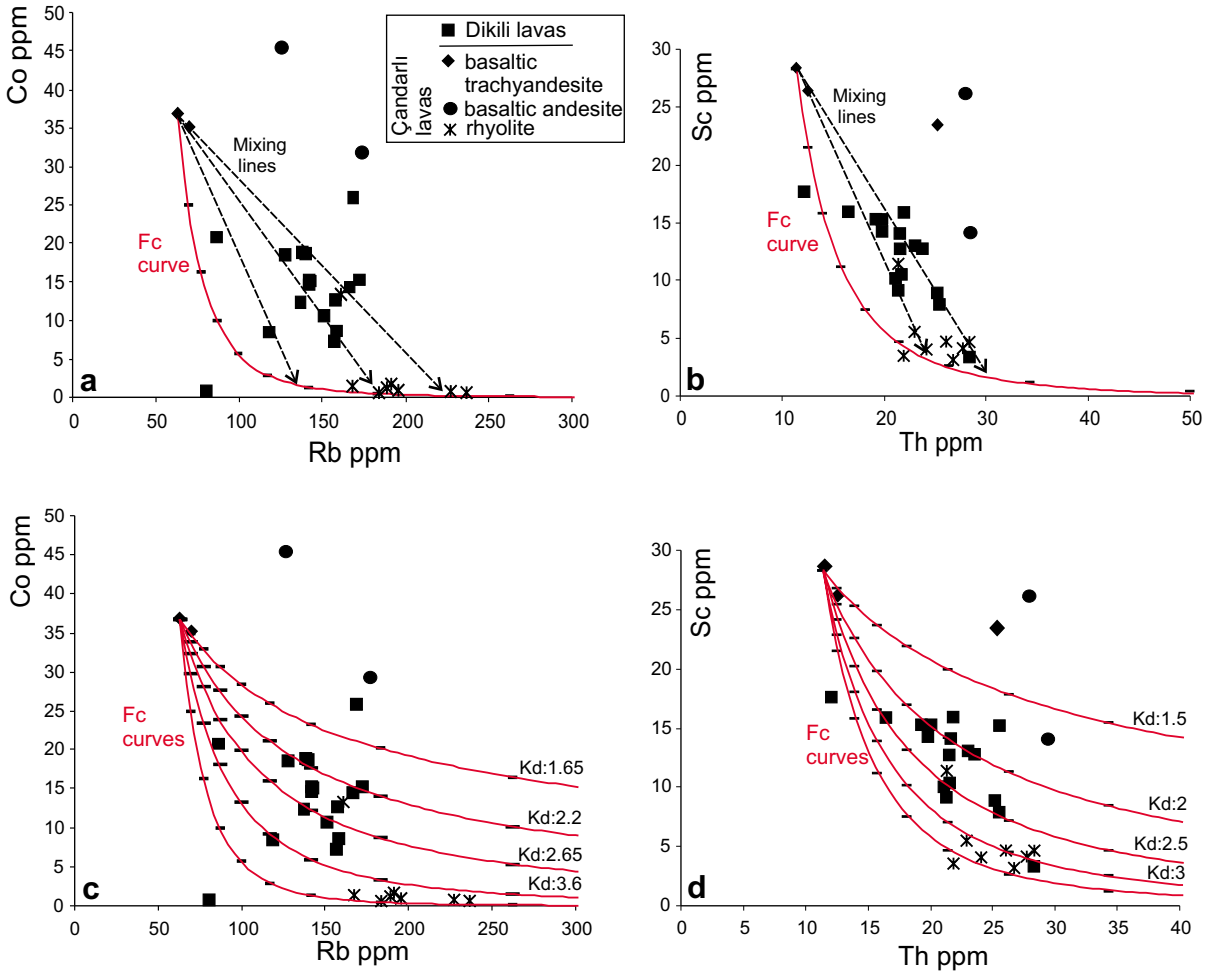

Figure 12. (a) Rb vs Co and (b) Th vs Sc diagrams for Dikili Çandarlı lavas. Tick marks on the fractional crystallization (FC) curves correspond to 10% crystallization intervals. Kd_{Rb}= 0.043, Kd_{Th}= 0.075, Kd_{Co}= 4.65 and Kd_{Sc}= 3.6 (c) Rb vs Co and (d) Th vs Sc diagrams for Dikili Çandarlı lavas with additional FC curves are calculated with decreasing Kd_{Rb} and Kd_{Th} values, respectively.

distinct Eu anomaly, related to extensive crystallization of plagioclase (Figure 13).

Multi-Element Patterns

N-type MORB normalized multi-element patterns of Dikili and Çandarlı lavas are shown in Figure 14. All volcanic units exhibit similar multi-element patterns characterised by significant enrichment in LILE (Large Ion Lithophile Elements; Rb, Ba, Th, U) and LREE relative to the high field strength elements Ta, Nb, Zr, Hf, Ti, Y and HREE. Incompatible elements including Tb, Yb, Y and especially Ti generally have values less than MORB. Acidic samples of the Çandarlı lavas have significant negative anomalies of Ba, Zr and Ti. Basaltic andesitic lavas of the Çandarlı group represent the similar pattern with the Dikili group but BTA is more enriched in Nd, Hf, Sm and Ti. Although there are some differences in Çandarlı BTA the patterns of Dikili-Çandalı lavas are closely similar to subduction-related active continental margin patterns of Pearce (1983). The enrichment in LILE and LREE relative to HFSE can indicate derivation from a mantle enriched by a subduction component mainly characterised by negative Nb and Ta anomalies and high Ba/Nb ratio. The selective

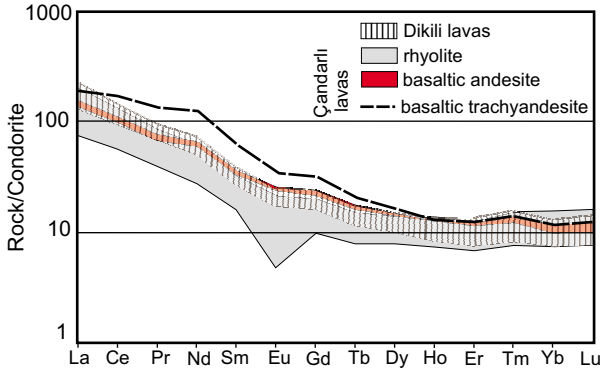

Figure 13. Chondrite-normalized REE patterns of lavas from Dikili-Çandarlı volcanics. Normalizing ratios are from Sun & Mc Donough (1989).

enrichment of the K, Rb, Th, Ba suggests the role of a superimposed crustal contamination following the derivation of the magma from its source region.

Previous studies indicate that the calc-alkaline Early–Middle Miocene volcanism of Western Anatolia seem to have the characteristics of collision-related, calc-alkaline and shoshonitic magmas (Güleç 1991; Aldanmaz *et al.* 2000). This magmatism derived from the lithospheric mantle beneath Western Anatolia carries a subduction component, which is characterized by negative Nb and Ta anomalies. On the other hand, alkaline Late Miocene–Pliocene volcanism represents OIB-like trace element patterns, derived from mainly asthenospheric mantle with less amount of lithospheric component and this volcanism indicates the presence of extensional regime (Güleç 1991; Seyitoğlu *et al.* 1997; Aldanmaz *et al.* 2000; Aldanmaz 2002; Alıcı *et al.* 2002). Geochemical features of the alkaline BTA dykes are very different from young alkaline volcanism of western Anatolian, as already mentioned in previous sections. The main differences are high MgO (12%) and K_2O (4%) content of BTA dykes. With these features, BTA is similar to the ultrapotassic lavas of the Bodrum area (Late Miocene), USE (Uşak-Selendi-Emet) area (Middle Miocene) and Dikili lavas of the Aldanmaz *et al.* (2000). Ultrapotassic rocks of the Bodrum peninsula have petrological and geochemical characteristics of primary mantle-derived magmas and their LIL element and initial isotopic compositions are evidence for the existence of the enriched mantle component (Robert *et al.* 1992). Seyitoğlu *et al.* (1997) claim that the USE lavas were derived from heterogeneously enriched subcontinental

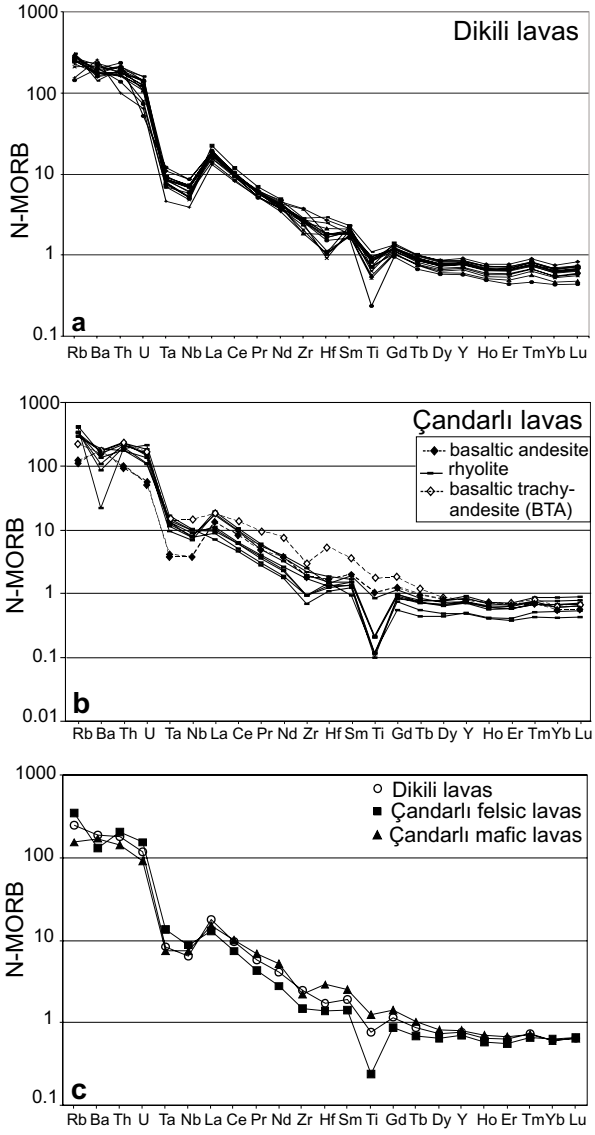

Figure 14. MORB-normalized trace elements patterns of **(a)** Dikili, **(b)** Çandarlı lavas and **(c)** for the average values from the Dikili-Çandarlı lavas. Normalization values are taken from Sun & Mc Donough (1989) and ordered by Pearce (1983).

lithosphere. This lithospheric mantle was enriched to varying degrees by subduction-related processes and/or small degree melts of depleted upper mantle (asthenosphere). Such enriched lithospheric mantle could have melted by decompression after only a small degree of extension in the Miocene (Yılmaz 1989; Seyitoğlu *et al.* 1997).

Discussion

The Dikili-Çandarlı volcanic complex presents an example of spatial coexistence of eruption products, which belong to different stages of magma chamber evolution. The first stage is 15–18 Ma (Borsi *et al.* 1972; Benda *et al.* 1974; Aldanmaz *et al.* 2000) in age and represented by pyroclastic deposits and andesitic, dacitic lavas which are strongly affected by magma mixing processes. The second stage consists of contemporaneous felsic and mafic lavas but there is no age determination from the lavas. However, correlations with similar lavas around the study area and relationships with the sedimentary rocks suggest a Late Miocene age (Borsi *et al.* 1972; Ercan *et al.* 1995; Aldanmaz *et al.* 2000).

The magmas of the Dikili-Çandarlı region are likely to have developed in an open system involving fractionation and mafic magma replenishment. Mixing of mafic and felsic magmas is also required for some rock types and is supported by disequilibrium phenocryst assemblages in andesite and dacite. Many of the crystals were out of equilibrium with their host magma. This kind of mineral assemblages can be seen in a single sample, such as Mg-rich olivine, reversely zoned orthopyroxene with Fe-rich cores and Mg-rich rims, and reversely zoned plagioclase with andesine cores and labradorite rims. The highly porphyritic nature of many of the lavas is also evidence for crystal accumulation (cf. Seaman 2000).

Elevated compatible element (e.g., Ni) concentrations at particular silica content in andesite were apparently produced by mixing of basalt and rhyolite magmas. In addition to these magma-mixing textures, mafic xenoliths, xenocrysts and replenishment textures are very common in these lavas. Plagioclase reaction textures also provide some evidence for this process. Numerous petrographic and experimental studies have suggested that a fritted or sieve texture in plagioclase results from the reaction of sodic crystals with a more calcic composition (cf. Kuno 1950; Anderson 1976; Lofgren & Norris 1981; Tsuchiyama 1985; Nixon & Pearce 1987; Glazner *et al.* 1990). As described in Stimac & Pearce (1992) zoning and reaction textures of plagioclase indicate that fritting occurs when sodic plagioclase was assimilated by hybrid magmas formed during the initial stages of mafic-felsic magma interaction. This intermediate magma rapidly loses heat as it is hybridized with adjacent silicic magma and crystallizes abundant plagioclase and pyroxene, eventually forming partially quenched inclusions. Alternatively, some authors have suggested that a fritted texture may form in plagioclase by rapid growth during episodes of undercooled crystallization (cf. Hibbard 1981; Anderson 1984). Kuo & Kirkpatrick (1982) described fritted crystals compatible with both origins. Textural and compositional relations in Dikili lavas indicate that fritted textures have formed by the reaction of sodic plagioclase derived from the silicic end-member with a more calcic melt composition.

The zoning pattern and compositional range of calcic cores of plagioclase phenocrysts in Dikili lavas is consistent with crystallization from basaltic andesite. There are several quenched andesitic inclusions, rich in pyroxenes, and angular pyroxene cumulates in dacites. As crystallization proceeds and the viscosity of inclusions and host become similar, inclusions suffer extensive disaggregation, contributing crystalline debris and hybrid liquid to dacite. Partially resorbed quartz phenocrysts with clinopyroxene rims are very common in andesite and basaltic andesite of Dikili lavas. We interpret such coronas as forming by diffusion-controlled growth of clinopyroxene in dissolution boundary layers on quartz. A similar process and consequences were described by Clynne (1999) for the Lassen Peak 1915 eruption products, which also involved mixing between silicic and mafic magmas (Tepley *et al.* 1999).

The effect of intrusion of hot magma into a cooler magma reservoir is widely recognized as a potential eruption trigger (e.g., Sparks *et al.* 1977; Pallister *et al.* 1992; Eichelberger 1995). Four different explosion stages and interrelated widespread pyroclastic deposits in the Dikili group (see the section Geologic Setting-Dikili group) can also indicate that this kind of lava mixing triggered the eruptions. The crystal-rich nature of the andesite and the low temperatures are interpreted in terms of a long-lived, relatively cool magma chamber. Periodic intrusion of mafic magma results in repeated remobilization of the resident magma. The most silicic dacite (SiO_2 68.06%) approaches the composition of the silicic end member.

Whole rock geochemical studies indicate that the fractional crystallization (FC) is not only the mechanism for the evolution of the Dikili lavas. Petrogenetic models, which are based on trace element variations, also indicate that the magma mixing processes were affective during the evolution of the volcanism.

Çandarlı volcanics, basalt and rhyolite, are the product of bimodal volcanism. Mafic lava groups mainly erupted at fissures as a dike and felsic lavas produced several domes and related pyroclastic deposits. BTA is the most primitive rock group in the area, which may be considered as representative of the primary parental magma. On the other hand, the rhyolitic magma rapidly ascended to the surface through the faults without noticeable crystallization in the transient chambers. The appearance of obsidians with extremely high content of SiO_2 (80.98%) is related to the formation of anhydrous high-temperature melts.

Conclusion

Dikili-Çandarlı volcanics are geochemically similar to high-K Miocene volcanic rocks of Western Anatolia. On the basis of petrologic studies, age determinations and tectonic settings, Miocene volcanism in the Western Anatolia are post collisional in nature and has a signature of a subduction component. Previous authors propose a subduction-related mantle origin for the melts and evolution through fractional crystallization and assimilation of crustal material (e.g., Innocenti *et al.* 1982; Yılmaz 1989; Güleç 1991; Aldanmaz *et al.* 2000). On the other hand, Upper Miocene–Pliocene alkaline lavas are different from previous stage and mainly related to extensional regime. This magmatism was generated by variable degrees of partial melting of an isotopically homogeneous mantle source that was enriched relative to depleted MORB mantle and primitive mantle (Güleç 1991; Aldanmaz 2002; Aldanmaz *et al.* 2000).

Calc alkaline, high-K Dikili lavas belong to first group, which are produced by stratovolcano explosive eruption products intercalated with pyroclastic deposits, flows breccias and lahar flows. Petrography as well as petrologic modeling and crystal chemistry indicate that magma mixing is the dominant processes for the generation of this group. So, there is unequivocal evidence for open-system behavior with influx of mafic magma into a crystal-rich andesite host. Crystals in the andesite record a complex history of growth and resorption that indicates basaltic andesite intruded dacite magma and is partially hybridised with. Mineral compositions of pyroxenes in the Dikili lavas indicate crystallization temperatures of 900–1150 °C for andesites and 700–1100 °C for dacites.

Bimodal Çandarlı lavas crop out along the two sets of oblique-slip normal faults trending NE–SW and NW–SE which delimit the Çandarlı depression. According to tectonic evolution of the region, these faults were formed by the effects of the extensional regime during the Late Miocene–Pliocene. Although Çandarlı mafic and felsic lavas are younger than the Dikili lavas, they present similar petrological features with Dikili lavas. Thus, Çandarlı lavas might be a late stage product of the Dikili lavas and/or transitional position between them. Beside this, BTA dikes of the Çandarlı group are the most primitive lavas of the region which is alkaline and ultrapotassic. Given that the Çandarlı lavas are younger than Dikili lavas, the nature of the BTA dikes points to periodic replenishment of the magma chamber with new influx of more primitive magma.

In conclusion, Dikili lavas were derived mainly from collision-related magmas which have subduction-related geochemical imprint, but mixing of mafic and felsic magmas in the upper crustal layers seems to have governed the composition of the Dikili lavas. Except BTA dike, Çandarlı lavas exhibit similar features to those of the Dikili lavas. The BTA is the most primitive lavas of the region which were derived from primitive magma batches that ascended rapidly from their sources.

Acknowledgements

We thank Iain McDonald for ICP-MS analysis as well as Peter Fisher for SEM studies. Ursula Robert provided helpful comments to improve this manuscript. We appreciate comments on the manuscript made by Nilgün Güleç, Ercan Aldanmaz and Erdin Bozkurt (Editor).

References

AKAY, C. 2003. Mineralogy and geochemistry of melilite leucitites, Balçıkhisar, Afyon Turkey). *Turkish Journal Earth Sciences* **12**, 215–239.

AKYÜREK, A. & SOYSAL, Y. 1983. Biga yarımadası güneyinin (Savaştepe-Kırkağaç-Bergama-Ayvalık) temel jeoloji özellikleri [Geological characteristics of south of Biga peninsula (Savaştepe-Kırkağaç-Bergama-Ayvalık)]. *Mineral Research and Exploration Institute (MTA) of Turkey Bulletin* **95/96**, 1–12 [in Turkish with English abstract].

ALDANMAZ, E. 2002. Mantle source characteristics of alkali basalts and basanites in an extensional intracontinental plate setting, western Anatolia, Turkey: implication for multi-stage melting. *International Geology Review* **44**, 440–457.

ALDANMAZ, E. 2006. Mineral-chemical constraints on the Miocene calc-alkaline and shoshonitic volcanic rocks of western Turkey: disequilibrium phenocryst assemblages as indicators of magma storage and mixing conditions. *Turkish Journal Earth Sciences* **15**, 47–73.

ALDANMAZ, E., PEARCE, J.A., THIRLWALL, M.F. & MITCHELL, J.G. 2000. Petrogenetic evolution of Late Cenozoic, post-collision volcanism in western Anatolia, Turkey. *Journal of Volcanology and Geothermal Research* **102**, 67–95.

ALICI, P., TEMEL, A. & GOURGAUD, A. 2002. Pb-Nd-Sr isotope and trace element geochemistry of Quaternary extension-related alkaline volcanism: a case study of Kula region (western Anatolia, Turkey). *Journal of Volcanology and Geothermal Research* **115**, 487–510.

ANDERSON, A.T. 1976. Magma mixing: Petrologic process and volcanological tool. *Journal of Volcanology and Geothermal Research* **1**, 3–33.

ANDERSON, A.T. 1984. Probable relations between plagioclase zoning and magma dynamics, Fuego volcano, Guatemala. *American Mineralogist* **69**, 660–676.

AYDAR, E., BAYHAN, H. & GOURGAUD, A. 2003. The lamprophyres of Afyon stratovolcano, Western Anatolia, Turkey: description and genesis. *Comptes Rendus Geoscience* **335**, 279–288.

BENDA, L., INNOCENTI, F., MAZZUOLI, R., RADICATI, F. & STEFFENS, P. 1974. Stratigraphic and radiometric data of the Neogene in Northwest Turkey. *Zeitschrift der Deutschen Geologischen Gesellschaft* **125**, 183–193.

BORSI, S., FERRARA, G., INNOCENTI, F. & MAZZUOLI, R. 1972. Geochronology and petrology of recent volcanics in the Eastern Aegean sea. *Bulletin of Volcanology* **36**, 473–496.

CLYNNE, M.A. 1999. A complex magma mixing origin for rocks erupted in 1915 in, Lassen Peak, California. *Journal of Petrology* **40**, 105–132.

COX, K.G., BELL, J.D. & PANKHURST, R.J. 1979. *The Interpretation of Igneous Rocks*. George Allen & Unwin, Boston.

DEVINE, J.D., MURPHY, M.D., RUTHERFORD, M.J., BARCLAY, J., SPARKS, R.S.J., CARROLL, M.R., YOUNG, S.R. & GARDNER, J. 1998. Petrologic evidence for pre-eruptive pressure-temperature conditions and recent reheating, of andesitic magma erupting at the Soufriere Hills Volcano, Montserrat (W.I.). *Geophysical Research Letters* **25**, 3669–3672.

EDİGER, V.S., BATI, Z. & YAZMAN, M. 1996. Palynology of possible hydrocarbon source rocks of the Alaşehir-Turgutlu area in the Gediz graben (western Anatolia). *Turkish Association of Petroleum Geologists Bulletin* **92**, 94–112.

EICHELBERGER, J.C. 1975. Origin of andesite and dacite: evidence of mixing at glass Mountain in california and other circum Pasific volcanoes. *Geological Society of America Bulletin* **86**, 1381–1391.

EICHELBERGER, J.C. 1995. Silisic volcanism: ascent of viscous magmas from crustal reservoirs. *Annual Review of Earth and Planetary Science* **23**, 41–63.

ERCAN, T. & GÜNAY, E. 1984. Kuzeybatı Anadolu, Trakya ve Ege adalarındaki Oligo–Miyosen yağlı volkaniklerin gözden geçirilişi [A review of Oligocene–Miocene volcanics in NW Anatolia, Thrace and Aegean islands]. *Geological Society of Turkey Bulletin* **5**, 119–139 [in Turkish with English abstract].

ERCAN, T., SATIR, M., SEVİN, D. & TÜRKECAN, A. 1996. Batı Anadoludaki Tersiyer ve Kuvaterner yağlı volkanik kayaçlarda yeni yapılan radyoaktif yağ ölçümlerinin yorumu [Interpretation of new radiometric age determinations of Tertiary and Quaternary volcanic rocks of Western Anatolia]. *Mineral Research and Exploration Institute (MTA) of Turkey Bulletin* **119**, 103–112 [in Turkish with English abstract].

ERCAN, T., SATIR, M., STEINITZ, G., DORA, A., SARIFAKIOĞLU, E., ADIS, C., WALTER, H. J. & YILDIRIM, T. 1995. Biga yarımadası ile Gökçeada, Bozcaada ve Tavşan adalarındaki (KB Anadolu) tersiyer volkanizmasının özellikleri [The features of Tertiary volcanics of Biga Peninsula, Gökçeada, Bozcaada and Tavşan islands in NW Anatolia]. *Mineral Research and Exploration Institute (MTA) of Turkey Bulletin* **117**, 55–86 [in Turkish with English abstract].

ERCAN, T., TÜRKECAN, A., AKYÜREK, B., GÜNAY, E., ÇEVİKBAŞ, A., ATEŞ, M., CAN, B., ERKAN, M. & ÖZKİRİŞÇİ, C. 1984. Dikili-Bergama-Çandarlı (Batı Anadolu) yöresinin jeolojisi ve magmatik kayaçların petrolojisi [Geology and magmatic petrology of Dikili-Bergama-Çandarlı (West Anatolia) region]. *Bulletin of Geological Engineering* 47–59 [in Turkish with English abstract].

ERKÜL, F., HELVACI, C. & SÖZBİLİR, H. 2005a. Stratigraphy and geochronology of the Early Miocene volcanic units in the Bigadiç borate basin, Western Turkey. *Turkish Journal Earth Sciences* **14**, 227–253.

ERKÜL, F., HELVACI, C. & SÖZBİLİR, H. 2005b. Evidence for two episodes of volcanism in the Bigadic borate basin and tectonic implications for western Turkey. *Geological Journal* **40**, 545–570.

EWART, A. 1979. A review of the mineralogy and chemistry of Tertiary–Recent dacitic, rhyolitic and related salic volcanic rocks. *In*: BARKER, F. (ed), *Trondhjemites, Dacites, and Related Rocks*. Amsterdam: Elsevier; 13–121.

EWART, A. 1982. The mineralogy and petrology of Tertiary–Recent orogenic volcanic rocks: with special reference to the andesitic-basaltic compositional range. *In*: THORPE, R.S. (ed), *Andesites: Orogenic Andesites and Related Rocks*. New York: John Wiley; 25–95.

FOLEY, S.F., VENTURELLI, G., GREEN, D.H. & TOSCANI, L. 1987. The ultrapotassic rocks: Characteristics, classification and constrains for petrogenetic models. *Earth Science Review* **24**, 81–134.

FRANCALANCI, L., INNOCENTI, F., MANETTI, P. & SAVAŞÇIN, Y. 2000. Neogene alkaline volcanism of the Afyon-Isparta area, Turkey: petrogenesis and geodynamic implications. *Mineralogy and Petrology* **70**, 285–312.

GENÇ, Ş.C., ALTUNKAYNAK, Ş., KARACIK, Z., YILMAZ, Y. & YAZMAN M. 2001. The Çubukludağ Graben, Karaburun peninsula: its tectonic significance in the Neogene geological evolution of the western Anatolia. *Geodinamica Acta* **14**, 45–55.

GENÇ, Ş.C. & YILMAZ, Y. 2000. Aliağa dolaylarının jeolojisi ve genç tektoniği [Geology and young tectonics of the Aliağa region]. *The Symposia on the Earthquake Possibility of Western Anatolia, İzmir*, 152–159 [in Turkish with English abstract].

GLAZNER, A.F., USSLER, W. & MATHIS, A.C. 1990. Interpretation of plagioclase texture in volcanic rocks. *EOS* **71**, p.1678.

GÜLEÇ, N. 1991. Crust-mantle interaction in western Turkey: implications from Sr and Nd isotope geochemistry of Tertiary and Quaternary volcanics. *Geological Magazine* **128**, 417–435.

HAMMARSTROM, J.M. & ZEN, E. 1986. Aluminium in hornblende: an empirical igneous Geobarometer. *American Mineralogist* **71**, 1297–1313.

HIBBARD, M.J. 1981. The magma mixing origin of mantled feldspars. *Contributions to Mineralogy and Petrology* **76**, 158–170.

INNOCENTI, F., KOLIOS, N., MANETTI, P., RITA, F. & VILLARY, L. 1982. Acid and basic Late Neogene volcanism in central Aegean Sea: its nature and geotectonic significance. *Bulletin of Volcanology* **45**, 87–97.

IRVIN, T.N. & BARAGAR, W.R.A. 1971. A guide to the chemical classification of the common volcanic rocks. *Canadian Journal of Earth Sciences* **8**, 523–548.

İZTAN, H. & YAZMAN, M. 1990. Geology and hydrocarbon potential of the Alaşehir (Manisa) area, western Turkey. *Proceedings of an International Earth Sciences Congress on Aegean Regions, İzmir,* 327–338.

JAKES, P. & WHITE, A.R. 1972. Major and trace element abundance in volcanic rocks of orogenic areas. *Geological Society of America Bulletin* **83**, 29–40.

KARACIK, Z. & YILMAZ, Y. 1998. Geology of the ignimbrites and the associated volcano-plutonic complex of the Ezine area, northwestern Anatolia. *Journal of Volcanology and Geothermal Research* **85**, 251–264.

KARACIK, Z. & YILMAZ, Y. 2000. Volcanism of the Dikili-Çandarlı high and the surroundings, Western Anatolia. *International Earth Sciences Colloquium on the Aegean Region, İzmir-Dokuz Eylül University Engineering Faculty, Department of Geology, IESCA-2000,* Proceedings, 33–38.

KAYA, O. 1981. Miocene reference section for the coastal parts of West Anatolia. *Newsletter on Stratigraphy* **10**, 164–191.

KELLER, J. 1983. Potassic lavas in the orogenic volcanism of the Mediterranean area. *Journal of Volcanology and Geothermal Research* **18**, 321–336.

KOZAN, T.A., ÖĞDÜM, F., BOZBAY, B., BIRCAN, A,. KEÇER, M., TÜFEKÇİ, K,. DURUKAL, A., DURUKAL, S., OZANER, S. & HERECE, M. 1982. *Burhaniye (Balıkesir)-Menemen (İzmir) Arası Kıyı Bölgesinin Jeomorfolojisi [Geomorphology of Coastal Region Between Burhaniye (Balıkesir)-Menemen (İzmir)]*. Mineral Research and Exploration Institute (MTA) of Turkey, Report no. **7287** [in Turkish, unpublished].

KRUSENSKY, R.D. 1976. Neogene calc-alkaline extrusive rocks of the Karalar-Yeşiller areas, Nortwest Anatolia, Turkey. *Bulletin of Volcanology* **40**, 336–360.

KUNO, H. 1950. Petrology of Hakone volcano and adjacent areas, Japan. *Geological Society of American Bulletin* **61**, 957–1020.

KUO, L.C. & KIRKPATRICK, R.J. 1982. Pre-eruption history of phyric basalts from DSDP Legs 45 and 46: Evidence from morphology and zoning patterns in plagioclase. *Contributions to Mineralogy and Petrology* **79**, 13–27.

LANGMUIR, C.H, VOCKE, R.D, HANSON, G.H & HART, S.R. 1978. A general mixing equation with applications to Icelandic basalts. *Earth and Planetary Science Letters* **37**, 380–392.

LEAKE, E.B., WOOLLEY, A.R., ARPS, C.E.S., BIRCH, W.D., GILBERT, M.C., GRICE, J.D., HAWTHRONE, F.C., KATO, A., KISCH, H.J., KRIVOVICHEV, V.G., LINTHOUT, K., LAIRD, J., MANDARINO, J A., MARESCH, W.V., NICKEL, E.H., ROCK, N.M.S., SCHUMACHER, J.C., SMITH, D.C., STEPHENSON, N.C.N., UNGARETTI, L., WHITTAKER, E.J.W. & GUO YOUZHI. 1997. Nomenclature of amphiboles: report of the Subcommittee on Amphiboles of the International Mineralogical Association, Commission on New Minerals and Mineral Names. *The Canadian Mineralogist* **35**, 219–246.

LE MAITRE, R.W. 1989. *A Classification of Igneous Rocks and Glossary of Terms,* 193. Blackwell, Oxford.

LINDSLEY, D.H. 1983. Pyroxene thermometry. *American Mineralogist* **68**, 477–493.

LINDSLEY, D.H. & ANDERSEN, D.J. 1983. A two pyroxene thermometer: Proceedings of the Thirteenth Lunar and Planetary Science Conference, Part 2. *Journal of Geophysical Research* **88** Supplement, A887–906.

LOFGREN, G.E. & NORRIS, P.N. 1981. Experimental duplication of plagioclase sieve and overgrowth textures. *Geological Society of America Abstracts with Programs* **13**, p. 498.

MURPHY, M.D, SPARKS, R.S.J., BARCLAY, J., CARROLL, M.R. & BREWER, T.S. 2000. Remobilization of andesite magma by intrusion of mafic magma at the Soufriere Hills Volcano, Montserrat, est Indies. *Journal of Petrology* **41**, 21–42.

NIXON, G.T. & PEARCE, T.H. 1987. Laser-interferometry study of oscillatory zoning in plagioclase: The record of magma mixing and phenocrysts recycling in calc-alkaline magma chambers, Iztaccihuatl volcano, Mexico. *American Mineralogist* **72**, 1144–1162.

NYE, C.J. & REID, M.R. 1986. Geochemistry of primary and least fractionated lavas from Okmok volcano, central Aleutians: implications for arc magma genesis. *Journal of Geophysical Research* **91 (B10)**, 10271–10287.

ÖNGÜR, T. 1972. *Dikili-Bergama Jeotermal Araştırma Sahasına İlişkin Jeoloji Raporu [Geological Report on Geothermal Field of Dikili-Bergama Region]*. Mineral Research and Exploration Institute (MTA) of Turkey, Report no. **5444** [in Turkish, unpublished].

PALLISTER, J.S, HOBLITT. R.P. & REYES, A.G. 1992. A basalt trigger for the 1991 eruptions of Pinatubo Volcano. *Nature* **356**, 426–428.

PEARCE, J.A. 1983. Role of subcontinental lithosphere in magma genesis at active continental margins. *In*: HAWKESWORTH, C.J. & NORRY, M.J. (eds), *Continental Basalt and Mantle Xenoliths.* Cheshire: Shiva Publishing Limited; 230–249.

ROBERT, U., FODEN, J. & VARNE, R. 1992. The Dodecanese Province, SE Aegean: A model for tectonic control on potassic magmatism. *Lithos* **28**, 241–260.

ROLLINSON, H R. 1993. *Using Geochemical Data: Evaluation, Presentation, Interpretation.* Wiley & Sons, Inc., New York.

SAVAŞÇIN, M.Y. 1990. Magmatic activities of Cenozoic compressioal and extensional tectonic regimes in Western Anatolia. *International Earth Science Congress on Aegean Region, 1990 Proceedings* **2**, 421–434.

SAVAŞÇIN, Y., FRANCALANCI, L., INNOCENTI, F., MANETTI, P., BIRSOY, R. & DAĞ, N. 1995. Miocene–Pliocene potassic ultrapotassic volcanism of the Afyon-Isparta region (central-western Anatolia-Turkey): petrogenesis and geodynamic implication. *In*: PIŞKİN, Ö., ERGÜN, M., SAVAŞÇIN, M.Y. & TARCAN, G. (eds), *International Earth Science Colloquium on the Aegean Region (IESCA) Proceedings* II, 487–502.

SEAMAN, S.J. 2000. Crystal clusters, feldspar glomerocrysts, and magma envelopes in the Atascosa Lookout lava flow, Southern Arizona, USA: recorders of magmatic events. *Journal of Petrology* **41**, 693–716.

ŞENGÖR, A.M.C. & YILMAZ, Y. 1981. Tethyan evolution of Turkey: a plate tectonic approach. *Tectonophysics* **75**, 181–241.

SEYİTOĞLU, G., ANDERSON, D., NOWELL, G. & SCOTT, B. 1997. The evolution from Miocene potassic to sodic Quaternary magmatism in Western Turkey: implications for enrichment processes in the lithospheric mantle. *Journal of Volcanology and Geothermal Research* **76**, 127–147.

SIMKIN, T. & SMITH, J.V. 1970. Minor-element distribution in olivine. *Journal of Geology* **78**, 304–325.

SİYAKO, M., BÜRKAN, K.A. & OKAY, A.İ. 1989. Biga ve Gelibolu yarımadalarının Tersiyer jeolojisi ve hidrokarbon olanakları [Hydrocarbon potential and geology of Tertiary rocks of Biga and Gelibolu peninsulas]. *Turkish Association of Petroleum Geologists Bulletin* **1**, 183–199 [in Turkish with English abstract].

SPARKS, R.S.J., SIGURDSSON, H. & WILSON, L. 1977. Magma mixing: a mechanism for triggering acid explosive eruptions. *Nature* **267**, 315–318.

STEWARD, M.L. & FOWLER, A.D. 2001. The nature and occurrence of discrete zoning in plagioclase from recently erupted andesitic volcanic rock, Montserrat. *Journal of Volcanology and Geothermal Research* **106**, 243–253.

STIMAC, J.A. & PEARCE, T.H. 1992. Textural evidence of mafic-felsic magma interaction in dacite lavas, Clear lake, California. *American Mineralogist* **77**, 795–809.

SUN, S.S. & MC DONOUGH, W.F. 1989. Chemical and isotopic systematic of oceanic basalts: Implications for mantle composition and processes, *In:* SAUNDERS, A.D. & NORRY, M.J. (eds), *Magmatism in the Ocean Basins.* Geological Society, London, Special Publications **42**, 313–345.

TEPLEY, F.J., DAVIDSON, J.P. & CLYNNE, M. A. 1999. Magmatic interactions as recorded in plagioclase phenocrysts of Chaos Crags, Lassen Volcanic center, California. *Journal of Petrology* **40**, 787–806.

TOKÇAER, M., AGOSTINI, S. & SAVAŞÇIN, M.Y. 2005. Geotectonic setting and origin of the youngest Kula volcanics (western Anatolia), with a new emplacement model. *Turkish Journal Earth Sciences* **14**, 145–166.

TSUCHIYAMA, A. 1985. Dissolution kinetics of plagioclase in the melt of the system diopside-albite-anorthite, and origin of dusty plagioclase in andesites. *Contributions to Mineralogy Petrology* **89**, 1–16

WILSON, M. 1989. *Igneous Petrogenesis*: A global tectonic approach. Kluwer, Dordrect.

YAVUZ, F. 2007. WinAmphcal: A Windows program for the IMA-04 amphibole classification. *Geochemistry Geophysics Geosystems* **8**, Q01004, doi:10.1029/2006GC001391.

YILMAZ, Y. 1989. An approach to the origin of young volcanic rocks of western Turkey. *In*: ŞENGÖR, A.M.C. (ed), *Tectonic Evolution of the Tethyan Region.* Kluwer; 159–189.

YILMAZ, Y., GENÇ, Ş.C., GÜRER, F., BOZCU, M., YILMAZ, K., KARACIK, Z., ALTUNKAYNAK, Ş. & ELMAS, A. 2000. When did the western Anatolian grabens begin to develop? *In:* BOZKURT, E., WINCHESTER, J.A. & PIPER, J.D.A (eds), *Tectonic and Magmatism in Turkey and Surrounding Area.* Geological Society, London, Special Publications **173**, 353–384.

YILMAZ, Y., GENÇ, Ş.C, KARACIK, Z. & ALTUNKAYNAK, Ş. 2001. Two contrasting magmatic associations of NW Anatolia and their tectonic significance. *Journal of Geodynamics* **31**, 243–271.

YÜCEL-ÖZTÜRK, Y., HELVACI, C. & SATIR, M. 2005. Genetic relations between skarn mineralization and petrogenesis of the Evciler Granitoids, Kazdağ, Çanakkale, Turkey and comparison with World Skarn Granitoids. *Turkish Journal Earth Sciences* **14**, 255–280.

Received 04 August 2006; revised typescript received 02 February 2007; accepted 23 February 2007